

LIQUIDS AS DESCRIBED BY QUANTUM AND CLASSICAL MECHANICS

PH.D. THESIS BY

THOMAS MOSTRUP NYMAND



DEPARTMENT OF CHEMISTRY

DENMARK

2000

To my family, Rikke, Esben and Gustav

Contents

List of papers	3
Introduction	5
Parameterized interaction potentials	9
II.1 The acquisition of potential parameters	10
II.2 Intermolecular perturbation theory	12
Molecular simulation methods	17
III.1 Statistical mechanics	17
III.2 Molecular dynamics simulation	20
III.3 Monte Carlo simulation	22
III.4 Long-range interactions	24
III.5 Molecular simulation on parallel computers	26
Chemical reactions in solution	29
IV.1 Reaction rate constants described by non-equilibrium statistical mechanics . .	29
IV.2 Simulation of an S_N2 reaction in aqueous micro-solution	32
IV.3 An entire reaction coordinate method	33
Properties of solvated molecules	39
V.1 A microscopic, perturbational solvent model	40
V.1.1 Molecular property derivatives	42
V.2 Chemical shifts of liquid water	43
V.3 The geometry of the water molecule in liquid water	44
V.4 The refractive index of liquid water	44
V.5 Summary	45
Applications to liquid properties	47
VI.1 Long-range interactions in polarizable liquid water	47
VI.1.1 The effect of boundary conditions on electric field and field-gradient .	48
VI.2 A comparative study of effective and polarizable potentials.	50
VI.3 The dielectric function of benzene	51

Acknowledgments**53**

List of papers

- PAPER I Dynamical Model for S_N2 Reactions in Microsolution:
The $Cl^- + CH_3Cl \rightarrow ClCH_3 + Cl^-$ Reaction.
Molecular Dynamics Simulation of Reaction Clusters
T. M. Nymand, K. V. Mikkelsen, P.-O. Åstrand, and G. D. Billing
Acta Chem. Scand., **53** 1043-1053 (1999)
- PAPER II Chemical shifts in liquid water calculated by molecular dynamics
simulations and shielding polarizabilities
T. M. Nymand, P.-O. Åstrand, and K. V. Mikkelsen
J. Phys. Chem. B, **101** 4105-4110 (1997)
- PAPER III Electric field-gradient contributions to the chemical shifts of liquid water
T. M. Nymand and P.-O. Åstrand
J. Chem. Phys., **106** 8332-8338 (1997)
- PAPER IV Calculation of the geometry of the water molecule in liquid water
T. M. Nymand and P.-O. Åstrand
J. Phys. Chem. A, **101** 10039-10044 (1997)
- PAPER V Refractive index of liquid water in different solvent models
K. O. Sylvester-Hvid, T. M. Nymand, P.-O. Åstrand, and K. V. Mikkelsen
J. Phys. Chem. A (accepted for publication)
- PAPER VI Ewald summation and reaction field methods for potentials
with atomic charges, dipoles, and polarizabilities
T. M. Nymand and P. Linse
J. Chem. Phys., **112** 6152-6160 (2000)
- PAPER VII Molecular dynamics simulations of polarizable water
at different boundary conditions
T. M. Nymand and P. Linse
J. Chem. Phys., **112** 6386-6395 (2000)

- PAPER VIII A comparison of effective and polarisable intermolecular potentials in simulations: Liquid water as a test case
T. M. Nymand, P. Linse, and P.-O. Åstrand
Mol. Phys. (submitted for publication)
- PAPER IX The temperature dependent dielectric function of liquid benzene. Interpretation of THz spectroscopy data by molecular dynamics simulation
T. M. Nymand, C. Rønne, and S. R. Keiding
J. Chem. Phys. (submitted for publication)

Publications not included in the thesis

1. The Structure of Nitromalonamide: A Combined Neutron-Diffraction and Computational Study of a Very Short Hydrogen Bond
G. K. H. Madsen, C. Wilson, T. M. Nymand, G. J. McIntyre, and F. K. Larsen
J. Phys. Chem. A, **103** 8684-8690 (1999)
2. A theoretical study of the electronic spectrum of water
O. Christiansen, T. M. Nymand, and K. V. Mikkelsen
J. Chem. Phys. (submitted for publication)
3. MOLSIM, a combined MC/MD/BD simulation program, v. 3.0.7
P. Linse, A. Wallqvist, P.-O. Åstrand, T. M. Nymand, V. Lobaskin, and F. Carlsson
Lund University, Sweden (2000)

I Introduction

The work presented in this thesis is devoted to the theoretical study of liquids and solutions by the combined efforts of quantum chemical and classical molecular simulation (MS) techniques. In recognition of chemistry as a fundamentally experimental science, the purpose of theoretical chemistry in general is to reproduce experimental results, aid the interpretation of these, and, ultimately, predict the outcome of future experiments. In contrast to many of the very sophisticated models devised by theoretical chemists, the concept of MS is very simple. But despite its simplicity, MS results have shown remarkable agreement with the outcome of a variety of experiments. This has encouraged their use in the process of rationalizing and interpreting these, a process greatly facilitated by the very rich and detailed information provided by such simulations.

The theoretical study of liquids and solutions is challenging. In the gas-phase molecules translate, rotate, and vibrate freely only interrupted by occasional collisions. Intermolecular interaction is virtually absent and as a consequence, many macroscopic gas properties are described perfectly adequate by the ideal gas equation. In the crystalline phase, crystal structure symmetry greatly simplifies the characterization of molecular interaction. Neither of these descriptions apply completely to the liquid phase; the increased density (relative to the gas-phase) requires a detailed description of molecular interaction, and the order of the crystal vanishes upon melting. Nevertheless, from the viewpoint of a chemist, a detailed understanding of liquids is of great importance, since the bulk of applied chemistry occur in solution. To that end, an understanding of liquid water in particular is essential.

Water plays the most prominent role in biological systems. Not only is it the solvent in which all the chemical processes of life occur, it also appears to be very active in the determination of bio-macromolecular conformation, as well as in the transport processes occurring through cell membranes. Equally intriguing is the fact that liquid water in a thermo-dynamic aspect is the most peculiar of solvents. Among many anomalies it exhibits a density maximum just below 4°C and 1 atm, it has a negative volume of melting, and when pressure is applied its viscosity decreases.¹ It is perhaps even more interesting that despite the vast amount of both experimental and theoretical research devoted to the study of liquid water, this utmost important substance is still far from well understood. In particular, no clear and complete connection between microscopic properties of the water molecule and the thermo-dynamical anomalies of the liquid has yet been made. However, there is general consensus that the *hydrogen bonds* so abundant in water are very important in the explanation of its anomalous properties. Liquid water has been studied by simulations ever since the birth of the

methodology,² and has over time been the subject of numerous publications. In particular, molecular dynamics simulation has been an important tool in the search of an explanation of the anomalies of water.³ When studying microscopic solvent models, water is thus often used as a benchmark: any model performing well for a liquid as strongly associated as water is highly likely to be useful.

From the most fundamental point of view, a liquid is nothing but a vast number of electrons and nuclei moving in space and in principle all of its properties can be determined from the solutions of the Schrödinger equation. The Schrödinger equation is the cornerstone of quantum mechanics, in the framework of which the liquid would be described by the interaction energy of the nuclei and electrons and their kinetic energy. Even a numerical solution to this equation is, however, not attainable for systems comprising more than a few particles; the solution for larger systems is facilitated only by the introduction of a number of approximations. For the chemist, the most important of these is the Born-Oppenheimer approximation,⁴ the introduction of which leads to a separation of the Schrödinger equation into a nuclear and an electronic part. The solution of the *electronic* Schrödinger equation, which is the primary workhorse of quantum chemistry, provides electronic energies depending parametrically on the relative positions of the nuclei. Further, the electronic energy takes the role as the potential energy in the *nuclear* Schrödinger equation. In other words, the motion of the nuclei - and hence chemical transitions - occurs on a *potential energy surface* determined by the solution of the electronic Schrödinger equation. Since the electronic energy governs the nuclear motion, it also determines the stable nuclear conformations, the molecules. The nuclear Schrödinger equation can be solved fully quantum mechanically for small systems or for larger systems by the application of semi-classical methods. Finally, the nuclear motion is in many cases approximated by classical mechanics, which is the basic assumption behind molecular dynamics simulation.

Self-evidently, the most central concept in the methodology of MS is that of the molecule. This concept is of course also absolutely fundamental in chemistry in general. In that context, molecules are regarded as consisting of atoms joined by *covalent bonds*. While the formal description of covalent bonding is provided by quantum chemistry via the electronic Schrödinger equation, a covalent bond is often simply characterized by the amount of energy required to break it; usually about 100 kcal/mol. A covalent bond is formed by an electron pair; each of the atoms participating in the bonding donate one of their outermost electrons - *valence electrons* - to the formation of the bond. The breaking and formation of covalent bonds thus changes the electron distribution of the molecule dramatically. In a quantum chemical context, the description of chemical reactions therefore requires a global treatment of the interacting species. The interactions dominating the liquid phase, are, on the other hand, of a much weaker character. The strongest type of *intermolecular interaction*, the hydrogen bond has a typical strength of ~ 20 kJ/mol. These interactions cause only a slight change in the electronic structure of the participating molecules. Hence, in contrast to the individual molecule requiring a complete quantum mechanical description accounting for the covalent bonds, intermolecular interactions may be treated as perturbations.

The development and application of MS methods as well as the construction of the required

intermolecular potentials, rely heavily on the use of modern computers. Theoretical chemistry appears to be one of only a handful of research fields in which the need for faster and larger computers will never be satisfied. The development and use of efficient computer programs is therefore an important part of the work of a theoretical chemist. In the field of MS it is particularly fruitful to pursue the development of parallel programs to benefit from the ongoing progress in the development of parallel architectures.

As I began my Ph.D. work, Kurt V. Mikkelsen encouraged me to investigate the chloride-methyl-chloride reaction in micro-solution by molecular dynamics simulation, a reaction previously studied by Billing and Mikkelsen in aqueous solution.⁵ This work is presented in Paper I and Chapter IV of the present thesis. In the early phase of that project, I was introduced to Dr. Per-Olof Åstrand. Besides from offering me outstanding supervision in the field of MS, he later suggested the application of the entire reaction coordinate method to this reaction. The outcome of this is described in Section IV.3. He also had a particular interest in attempting to model solvent effects on molecular properties by the use of perturbation theory, and we soon embarked on the project addressing nuclear magnetic shielding in liquid water. The intermolecular perturbation theory (IPT) model used in that work is the topic of Chapter V and Paper II. The description of the chemical shift was later improved by including an electric field-gradient contribution, presented in Paper III and Section V.2. We felt encouraged to further investigate the possibilities of the IPT model, which led to the study of the geometry of the water molecule in liquid water, treated in Paper IV and Section V.3. At that time I shared an office with Dr. Kristian O. Sylvester-Hvid, another of Mikkelsen's students. Along with Mikkelsen and Åstrand we initiated a study of the refractive index of water, employing the IPT model as well as other microscopic solvent models. This work is described in Paper V and Section V.4. During the same period I had become increasingly interested in the development of MS computer programs. Encouraged by Åstrand and Mikkelsen, I started a project concerning long-range interactions in polarizable systems with Dr. Per Linse, the primary author of the MOLSIM program.⁶ This topic is presented in Sections III.4 and VI.1. During several visits in Lund, Sweden, the fundament ultimately leading to Paper VI and VII was laid. In the course of this collaboration I also had the opportunity to initiate the parallelization of the MOLSIM program using MPI, as described in Section III.5. During that period of time, working with polarizable systems had caused a growing interest in their more general properties. Ultimately, this led to the investigation of an effective model for a polarizable potential, the topic of Paper VIII and Section VI.2.

During the last couple of years I have enjoyed the possibility of collaborating with different people in the local Laser Chemistry Group, sharing my interest in molecular dynamics of liquids. A recent project in cooperation with Cecilie Rønne and Dr. Søren R. Keiding concerning the dielectric loss function of benzene is presented in Paper IX and Section VI.3.

The outline of this thesis is as follows: Chapter II discusses the notion of parameterized interaction potentials or potential energy surfaces, as these provide the foundation for performing simulations. In Chapter III the basic methodology of MS is presented, along with the more specialized topics of long-range interactions and parallelism. The study of the chloride-methyl-chloride reaction is described in Chapter IV. The topic of Chapter V is the modeling

of molecular properties in solution. Here the IPT solvent model, as well as its applications are presented. Chapter VI summarizes the work concerning liquid properties.

II Parameterized interaction potentials

The cornerstone of molecular simulation is the interaction potential surfaces upon which molecular motion occurs. Disregarding the inherent limitations of treating the molecules classically, the quality of any result extracted from a simulation will ultimately be governed by the quality of the potential. The theory of intermolecular interaction in general and of parameterized interaction potentials in particular is essential when employing simulation methods.

Intermolecular interactions contain four fundamental physical contributions, the electrostatic, induction, dispersion, and exchange contributions. The interaction energy may be written as a sum of these

$$U_{inter} = U_{ele} + U_{ind} + U_{disp} + U_{exch} . \quad (\text{II.1})$$

Electrostatic or Coulombic interactions occur among molecules possessing permanent electric moments; charges, dipole-, quadrupole-, and higher-order moments. In such a system, the molecular charge distributions become polarized and interactions between induced and permanent moments account for the induction energy. Even in systems of particles lacking permanent electric moments instantaneous electric moments arise by fluctuations in the electron distribution. These moments are stabilized in the presence of other such moments, giving rise to the dispersion interaction. At short intermolecular distances, interactions from electron exchange between molecules become significant.

The general form of the potential energy determining the nuclear motion in a system of N molecules may be written

$$\begin{aligned} U = U_1 + U_{inter} &= U_1 + U_2 + U_3 + \dots + U_N \\ &= \sum_i^N U_i + \sum_{i>j}^N U_{ij} + \sum_{i>j>k}^N U_{ijk} + \dots + U_{1\dots N} , \end{aligned} \quad (\text{II.2})$$

where the first equality establishes the connection to Eq. II.1 and the first term on the right hand side of the last equality describes all intramolecular interactions, the second (two-body) term all interactions involving exactly two molecules, the third (three-body) term all interaction involving exactly three molecules, etc.

Since Eq. II.2 represents a solution to the electronic Schrödinger equation (as discussed in the introduction), the variables in this expression are the nuclear degrees of freedom. If the total number of atoms is M and $M > 2$ there are $3M - 6$ variables. A discrete or otherwise general treatment of a potential energy surface of these dimensions would be

completely intractable in a numerical application. When performing MS the dominating part of the computational effort is spent on repeating evaluations of the intermolecular energies and forces and therefore it is desirable to make those as efficient as possible. The interaction potentials used in simulations therefore approximate Eq. II.2 by a number of parameterized analytical functions known to have the correct physical form. The collection of such a set of analytical functions along with their parameters will constitute a complete potential model or just *potential*, directly aimed at the use in MS. In this representation the number of variables is drastically reduced for example by allowing the interaction energy of a given pair of atoms to depend only on their separation and not on the relative orientation of the molecules they belong to.

The vibrational motion of the molecules is described by the first term in Eq. II.2. The energetically strongest contributors are often the stretching modes of covalent bonds, conveniently described by Morse-type functions. At room temperature, the characteristic energy $\hbar\omega$ can for stretching modes be appreciably larger than $k_B T$ causing this motion to display a strong quantum mechanical character. This renders the inherently classical treatment problematic and many potential models completely neglect the intramolecular term, or include a description of bending and torsional motions only. Examples of the latter are the force fields utilized in simulations of proteins, such as GROMOS96.⁷

The two-body term is always present in a potential model. Often it is given as a sum over site-site or atom-atom interactions. Perhaps the most common example is the 1-6-12 potential[†]

$$U_{ij} = \sum_{a \in i, b \in j} \left\{ \frac{q_a q_b}{r_{ab}} + 4\epsilon_{ab} \left[\left(\frac{\sigma_{ab}}{r_{ab}} \right)^{12} - \left(\frac{\sigma_{ab}}{r_{ab}} \right)^6 \right] \right\} \quad (\text{II.3})$$

where the notation $a \in i$ indicates that site a belongs to molecule i . Here the first term represents the Coulomb interaction between site charges q_a and q_b , the second term models the exchange repulsion, and the third term the dispersion interaction. In comparison to Eq. II.1 the lack of a term modeling the induction energy is noted. This potential model dominates the force fields used in simulation programs.^{8,9} The combination of the r^{-6} and r^{-12} terms is known as the Lennard-Jones potential.

In many potential models, Eq. II.2 is truncated after the second (two-body) term. Higher-order terms are occasionally explicitly included but more often, many-body effects are treated by the inclusion of induction by assuming the molecules or atoms to be polarizable. Induction is the single most important many-body effect for polar molecules in the condensed phase, and contributes to all two-body and higher-order terms in Eq. II.2.

II.1 The acquisition of potential parameters

The characteristics of the simulated molecules enter the potential model via the *potential parameters*, e.g. q_a , σ_{ab} , and ϵ_{ab} in Eq. II.3. The methods available to assess potential parameters usually fall into either the empirical or the *ab initio* category distinguished by

[†]Unless explicitly stated otherwise, atomic units will be used throughout.

the nature of the information they apply in the determination of the parameters. Often both sources of data are used, rendering the potential semi-empirical.

Within an empirical approach, potential parameters are determined such that certain experimental macroscopic liquid properties are reproduced by simulation. A well known example is the SPC/E potential¹⁰ for water which was determined such as to reproduce the experimental density and vaporization energy at room temperature. Empirical potentials are often simple two-body potentials (SPC/E is a 1-6-12 potential) that nevertheless may produce simulation results in excellent agreement with experiments. This is of course self-evident for properties included in the parameterization but it is also important that the parameterization procedure allows for the two-body potential to partially model many-body effects in an average manner. For example, the dipole moment of the water molecule in liquid water is substantially larger than that of the isolated water molecule (1.8 D) due to induction. This behavior is imitated in the SPC/E potential in which the (permanent) dipole moment of the water molecule is 2.35 D. On the other hand, this deems the potential inadequate to model the behavior of a water surface where the dipole moment is expected to be closer to that of the gas-phase molecule,¹¹ and further questions its ability to model the solvation of other polar molecules.¹²

Alternatively, potential parameters may be obtained from quantum chemical *ab initio* data. In doing so, the biasing towards certain liquid properties is avoided and the predictive value of simulations is improved. Moreover, there should be no reason to expect the potential model to fail, when simulation conditions such as pressure and temperature extend the range within which the experimental data was gathered, as is the case for empirical potentials. Further, the determination of an interaction potential becomes a task completely isolated from that of improving the quality of simulation methods, e.g. by incorporating the treatment of long-range interactions (see Sections III.4 and VI.1). This is not the case for empirical potentials which strictly are only useful under simulation conditions similar to those applied when the potential parameters were fitted.¹³

The quantum chemical data applied in the construction of intermolecular potentials usually originate from either supermolecular or perturbation theory calculations. In the former approach, the interaction energies of a large number of molecular complexes are calculated using quantum chemical methods. The interaction energy of a molecular dimer can be calculated as

$$U = E - E_A - E_B \quad (\text{II.4})$$

where E is the total dimer energy and E_A and E_B are the energies of molecules A and B . Subsequently, these energies are fitted to analytical expressions such as Eq. II.3. In principle, the U_{ij} term of Eq. II.2 can be determined from interaction energies of a number of dimers, the U_{ijk} term from trimer interaction energies, etc. However, since the interaction energy is very small compared to the total molecular energies, these must be highly accurate. Due to the finite basis sets employed, problems are also encountered in terms of basis set super-position errors.¹⁴ Finally, the supermolecular approach provides no information of the magnitude of the various contributions in Eq. II.1, only the total interaction energy.

II.2 Intermolecular perturbation theory

The intermolecular perturbation theory (IPT) as developed by Stone *et al.*¹⁵ is a special case of symmetry adapted perturbation theory,¹⁶ and can be used to provide intermolecular potentials for use in simulations. The use of IPT is well described in the literature^{17–20} and will here be demonstrated for the Coulomb interaction.

The total electronic Hamiltonian for two interacting molecules is

$$\mathcal{H} = \mathcal{H}_A + \mathcal{H}_B + \mathcal{V}_{AB} , \quad (\text{II.5})$$

where the zeroth-order Hamiltonian is the sum of the Hamiltonians for molecules A and B , $\mathcal{H}_A + \mathcal{H}_B$, and \mathcal{V}_{AB} describes the Coulomb interaction between the two molecules. The wave functions of the individual molecules in their ground states are assumed to be known, i.e. $\mathcal{H}_A |\Psi_0^A\rangle = \epsilon_0^A |\Psi_0^A\rangle$ and $\mathcal{H}_B |\Psi_0^B\rangle = \epsilon_0^B |\Psi_0^B\rangle$. We will consider only the long-range limit of molecular interaction where the charge distributions of molecules A and B are non-overlapping. In that case the ground state of the zeroth-order wave function for the component system ($A + B$) may be written as a direct product

$$|\Psi_0^{(0)}\rangle = |\Psi_0^A \Psi_0^B\rangle \quad (\text{II.6})$$

assumed to be properly normalized. Rayleigh-Schrödinger perturbation theory^{21,22} can now be employed to obtain the total energy

$$E = E^{(0)} + E^{(1)} + E^{(2)} + \dots \quad (\text{II.7})$$

to various orders in the perturbation \mathcal{V}_{AB} . Since the zeroth-order energy is

$$E^{(0)} = \langle \Psi_0^{(0)} | \mathcal{H}_A + \mathcal{H}_B | \Psi_0^{(0)} \rangle = \epsilon_0^A + \epsilon_0^B , \quad (\text{II.8})$$

the interaction energy of Eq. II.4 can be identified as $E^{(1)} + E^{(2)} + \dots$, by assuming that the molecules are in their electronic ground-state, $E_A = \epsilon_0^A$ and $E_B = \epsilon_0^B$, that is. The interaction operator describing the Coulomb interaction of electrons in molecules A and B is

$$\mathcal{V}_{AB} = \sum_{i \in A} \sum_{j \in B} \frac{1}{|\mathbf{R}_j - \mathbf{R}_i|} = \sum_{i \in A} \sum_{j \in B} \frac{1}{|\mathbf{r}_j - \mathbf{r}_i + \mathbf{r}_{AB}|} , \quad (\text{II.9})$$

where summations run over electrons. The notation $i \in A$ indicates that electron i belongs to molecule A . \mathbf{R}_i is the position of electron i , $\mathbf{r}_{AB} = \mathbf{r}_A - \mathbf{r}_B$ the vector between the origins (e.g. center of mass) of the molecules, and \mathbf{r}_i the position of electron i with respect to the molecular origin (see Figure II.A). Since \mathbf{r}_i and \mathbf{r}_j are assumed to be small compared to \mathbf{r}_{AB} , \mathcal{V}_{AB} may be Taylor-expanded in \mathbf{r}_i and \mathbf{r}_j around $\mathbf{r}_i = \mathbf{r}_j = 0$. The terms in this series will contain one factor depending only on the wave function of molecule A , one factor depending only on molecule B , and one factor depending only on the relative position and orientation of molecules A and B .

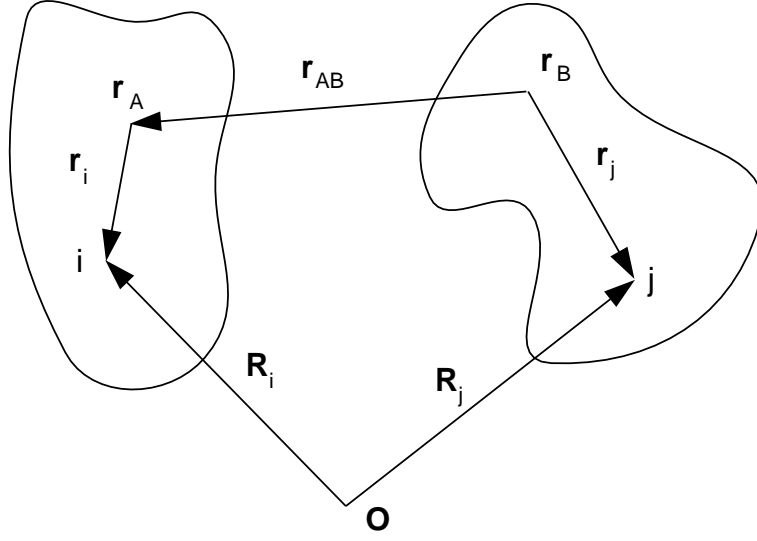


Figure II.A. Two interacting molecules A and B with origins \mathbf{r}_A and \mathbf{r}_B , respectively.

This means that when the first-order contribution to the energy is calculated according to

$$E^{(1)} = \langle \Psi_0^A \Psi_0^B | \mathcal{V}_{AB} | \Psi_0^A \Psi_0^B \rangle, \quad (\text{II.10})$$

the contributions to $E^{(1)}$ also factorize into two molecular factors and an interaction factor. The molecular terms can be identified as molecular electric moments, and the first-order energy contribution becomes[†]

$$\begin{aligned} E^{(1)} &= q_A T_{AB} q_B + q_A T_{AB}^\alpha \mu_{B,\alpha} - \mu_{A,\alpha} T_{AB}^\alpha q_B - \mu_{A,\alpha} T_{AB}^{\alpha\beta} \mu_{B,\beta} \\ &+ \frac{1}{3} q_A T_{AB}^{\alpha\beta} \Theta_{B,\alpha\beta} + \frac{1}{3} \Theta_{A,\alpha\beta} T_{AB}^{\alpha\beta} q_B - \frac{1}{3} \mu_{A,\alpha} T_{AB}^{\alpha\beta\gamma} \Theta_{B,\beta\gamma} \\ &+ \frac{1}{3} \Theta_{A,\alpha\beta} T_{AB}^{\alpha\beta\gamma} \mu_{B,\gamma} + \frac{1}{9} \Theta_{A,\alpha\beta} T_{AB}^{\alpha\beta\gamma\delta} \Theta_{B,\gamma\delta} + \dots, \end{aligned} \quad (\text{II.11})$$

the multipole expansion of the electrostatic energy.¹⁸ Here q_A , $\mu_{A,\alpha}$, and $\Theta_{A,\alpha\beta}$ are the charge, the α -component of the dipole moment, and the $\alpha\beta$ -component of the traceless quadrupole moment of molecule A , respectively, and the *interaction tensors* for site A and B are

$$\begin{aligned} T_{AB} &= r_{AB}^{-1} \\ T_{AB}^\alpha &= \nabla_\alpha T_{AB} = r_{AB,\alpha} r_{AB}^{-3} \\ T_{AB}^{\alpha\beta} &= \nabla_\alpha \nabla_\beta T_{AB} = (3r_{AB,\alpha} r_{AB,\beta} - r_{AB}^2 \delta_{\alpha\beta}) r_{AB}^{-5} \\ T_{AB}^{\alpha\beta\gamma} &= \nabla_\alpha \nabla_\beta \nabla_\gamma T_{AB} = [15r_{AB,\alpha} r_{AB,\beta} r_{AB,\gamma} \\ &\quad - 3r_{AB}^2 (r_{AB,\alpha} \delta_{\beta\gamma} + r_{AB,\beta} \delta_{\alpha\gamma} + r_{AB,\gamma} \delta_{\alpha\beta})] r_{AB}^{-7} \\ T_{AB}^{\alpha\beta\gamma\delta} &= \nabla_\alpha \nabla_\beta \nabla_\gamma \nabla_\delta T_{AB} = \dots, \end{aligned} \quad (\text{II.12})$$

etc. By introducing the infinitesimal test charge δq at \mathbf{r} , the electrostatic potential at \mathbf{r} is defined according to

$$\phi(\mathbf{r}) \equiv \lim_{\delta q \rightarrow 0} \frac{\partial U'}{\partial \delta q}, \quad (\text{II.13})$$

[†]We will conform to the Einstein summation convention for Greek letter indices throughout.

where U' is the potential energy $E^{(1)}$ of the system consisting of molecules A , B , and additional charge-moment terms describing the interaction between the test charge and the molecules. In turn, the α -component of the electrostatic field at \mathbf{r} is defined as

$$E_\alpha(\mathbf{r}) \equiv -\frac{\partial\phi(\mathbf{r})}{\partial r_\alpha} , \quad (\text{II.14})$$

and the $\alpha\beta$ -component of the electrostatic field gradient at \mathbf{r} as

$$E_{\alpha\beta}(\mathbf{r}) \equiv \frac{\partial E_\alpha(\mathbf{r})}{\partial r_\beta} . \quad (\text{II.15})$$

The result of applying the definitions II.13, II.14, and II.15, and evaluating the results at r_A yields the electrostatic potential

$$\phi_A = T_{AB}q_B + T_{AB}^\alpha\mu_{B,\alpha} + \frac{1}{3}T_{AB}^{\alpha\beta}\Theta_{B,\alpha\beta} + \dots , \quad (\text{II.16})$$

the field

$$E_{A,\alpha} = T_{AB}^\alpha q_B + T_{AB}^{\alpha\beta}\mu_{B,\beta} + \frac{1}{3}T_{AB}^{\alpha\beta\gamma}\Theta_{B,\beta\gamma} + \dots , \quad (\text{II.17})$$

and the field-gradient

$$E_{A,\alpha\beta} = -\left(T_{AB}^{\alpha\beta}q_B + T_{AB}^{\alpha\beta\gamma}\mu_{B,\gamma} + \frac{1}{3}T_{AB}^{\alpha\beta\gamma\delta}\Theta_{B,\gamma\delta} + \dots \right) , \quad (\text{II.18})$$

at molecule A due to the presence of molecule B . Eqs. II.16 through II.18 allow the electrostatic energy to be recast as

$$U_{ele} = q_A\phi_A - \mu_{A,\alpha}E_{A,\alpha} - \frac{1}{3}\Theta_{A,\alpha\beta}E_{A,\alpha\beta} = q_B\phi_B - \mu_{B,\alpha}E_{B,\alpha} - \frac{1}{3}\Theta_{B,\alpha\beta}E_{B,\alpha\beta} \quad (\text{II.19})$$

if moments higher than quadrupolar are neglected.

The second-order contribution to the energy is given as

$$E^{(2)} = \sum_{p+q>0} \frac{\langle \Psi_0^A \Psi_0^B | \mathcal{V}_{AB} | \Psi_p^A \Psi_q^B \rangle \langle \Psi_p^A \Psi_q^B | \mathcal{V}_{AB} | \Psi_0^A \Psi_0^B \rangle}{\epsilon_0^A - \epsilon_p^A + \epsilon_0^B - \epsilon_q^B} , \quad (\text{II.20})$$

which is readily obtained from the general expression for the second-order energy contribution of time-independent perturbation theory. The introduction of the dynamic dipole polarizability

$$\alpha_{\alpha\beta}(\omega) = \sum_{p>0} \left(\frac{1}{\omega_p + \omega} + \frac{1}{\omega_p - \omega} \right) \sum_{i,j} \langle \Psi_0 | r_{i,\alpha} | \Psi_p \rangle \langle \Psi_p | r_{j,\beta} | \Psi_0 \rangle , \quad (\text{II.21})$$

where $\omega_p = \epsilon_p - \epsilon_0$, of which the static dipole polarizability $\alpha_{\alpha\beta}$ is a special case ($\omega = 0$), allows terms in Eq. II.20 with $p = 0$ or $q = 0$ to be identified as the induction energy. These become

$$U_{ind} = -\frac{1}{2}\alpha_{A,\alpha\beta}E_{A,\alpha}E_{A,\beta} - \frac{1}{2}\alpha_{B,\alpha\beta}E_{B,\alpha}E_{B,\beta} \quad (\text{II.22})$$

provided the interaction operator \mathcal{V}_{AB} contains up to linear terms only in either $r_{i,\alpha}$ or $r_{j,\alpha}$ (the dipole approximation).

The remaining part of Eq. II.20, which will be identified as the dispersion energy is not straightforwardly separated into factors of molecular and interaction origin, since the denominator of terms with both $p > 0$ and $q > 0$ contains energies for both molecules. However, the use of an identity for this denominator yielding the desired factorization¹⁸ and the dipole approximation for \mathcal{V}_{AB} allows the dispersion energy to be written as

$$U_{disp} = -\frac{1}{2\pi} T_{AB}^{\alpha\gamma} T_{AB}^{\beta\delta} \int_0^\infty d\omega \alpha_{A,\alpha\beta}(i\omega) \alpha_{B,\gamma\delta}(i\omega) . \quad (\text{II.23})$$

By introducing the approximation $\alpha_{\alpha\beta}(i\omega) \approx \alpha_{\alpha\beta} \frac{\bar{\omega}^2}{\bar{\omega}^2 + \omega^2}$, equivalent to the approximation applied by London,^{23,24} we arrive at

$$U_{disp} = -\frac{1}{4} \frac{\bar{\omega}^A \bar{\omega}^B}{\bar{\omega}^A + \bar{\omega}^B} T_{AB}^{\alpha\gamma} T_{AB}^{\beta\delta} \alpha_{A,\alpha\beta} \alpha_{B,\gamma\delta} . \quad (\text{II.24})$$

Here $\bar{\omega}^A$ is interpreted as an average ionization energy of molecule A . When employed in simulations Eq. II.24 is often approximated by an isotropic term proportional to r^{-6} as in Eq. II.3.

It has been demonstrated that when IPT is applied for the Coulomb interaction of the electrons, the first-order energy contribution is the electrostatic energy and the two second-order contributions are the induction and dispersion energy terms. The important exchange repulsion term does not enter due to neglect of intermolecular charge distribution overlap[†] in Eq. II.6. However, it can be established by the Heitler-London method of exchange perturbation theory.²⁵

Thus, IPT readily provides the individual fundamental contributions to the interaction energy in Eq. II.1, thereby allowing for a more detailed analysis of the nature of intermolecular interactions. The discrimination between a hydrogen-bond and a pure dispersion, exchange interaction as in $\text{Ar} \cdots \text{Ar}$ is indeed possible by IPT, but formally not by the supermolecular approach. Moreover, simulation parameters as obtained by IPT are computed from quantum chemical calculations on the solute *monomer*, resulting in a modest computational load as compared to the supermolecular approach. Furthermore, the obtained parameters such as charges, dipole moments, and polarizabilities have an unambiguous physical interpretation which is not the case for parameters fitted to analytical expressions. Finally, the most important many-body effect, induction, is directly accounted for as shown above. The work presented in this thesis has greatly relied on potentials derived using intermolecular perturbation theory namely the so-called NEMO potentials.^{20,26–29} In particular, the simulations described in Papers II–V, VII and VIII employ a NEMO potential³⁰ for the description of liquid water.

[†]Formally, both exchange repulsion *and* overlap effects are neglected in this presentation, thus both contributions should be addressed by U_{exch} .

III Molecular simulation methods

With a suitable potential at hand we are in principle ready to begin exploring liquids and solutions by molecular simulation. However, the classical models will provide a vast amount of information which cannot be measured directly or even measured at all. A molecular dynamics simulation will for example readily provide instantaneous positions and velocities of all particles in the system. Conversely, experiments yield information about liquids not directly available from simulations such as the static dielectric constant of the liquid. The necessary link connecting microscopic data generated by simulations and macroscopic experimental observables is constituted by statistical mechanics. An introduction to important statistical mechanical concepts will therefore be given before the presentation of simulation methodologies.

Molecular simulation is very often realized by the use of either a molecular dynamics (MD) or a Monte Carlo (MC) method.^{8,31} MD has the advantage of offering the possibility to compute both dynamic and static properties of the simulated system, whereas only static properties are available from MC simulations. The great flexibility in the choice of the MC trial move, however, (see below) facilitates efficient simulation of a number of systems, ensembles, and processes which cannot easily be simulated by MD. The two techniques thus supplement each other well, together providing an indispensable tool in the exploration of a wide range of phenomena occurring in the condensed phase.

III.1 Statistical mechanics

Perhaps surprisingly, the laws of statistical mechanics are more readily derived by the use of a quantum mechanical formulation rather than a classical one. Here the former approach will be used to present the fundamentals of statistical mechanics. The presentation is based on that by Frenkel and Smit³¹ and Reif.³²

If we wish to give a statistical description of a situation, we must consider a very large, but finite, number \mathcal{N} of systems prepared similarly, an *ensemble* of systems. With respect to that particular ensemble, we may determine the probability of occurrence of a particular event simply by evaluating the fraction of systems in the ensemble in which the event occurred.

Suppose we have a macroscopic, quantum mechanical system composed of N particles enclosed in a container of volume V , and that this system has total energy E . The degeneracy of this system, i.e. the number of quantum mechanical eigenstates $|i\rangle$ satisfying $\mathcal{H}|i\rangle = E_i|i\rangle$ with E_i in the interval between E and $E + \delta E$, is denoted $\Omega(N, V, E)$. Since N for macroscopic

systems is of the order of Avogadro's number, $\Omega(N, V, E)$ is very, very large.[†] Suppose further, that this system is in *equilibrium*, i.e. that the probability of finding the system in any one state is independent of time. Absolutely central to statistical mechanics is *the fundamental postulate of equal a priori probabilities*. This states that an isolated system in equilibrium is equally likely to be in any of its accessible states.³² Consider now the isolated quantum mechanical system shown in Figure III.A. The system is composed of two subsystems, which are allowed to interchange thermal energy, but not mechanical energy.

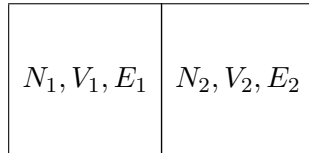


Figure III.A. A quantum mechanical system.

The Hamiltonian of this system can be written

$$\mathcal{H} = \mathcal{H}_1 + \mathcal{H}_2 + \mathcal{H}_{int} , \quad (\text{III.1})$$

where the two first terms are Hamiltonians for subsystems 1 and 2, respectively, and \mathcal{H}_{int} is the Hamiltonian describing their interaction. For the subsystems to interchange energy, this latter term must be non-vanishing, but we will assume that it is negligible compared to $\mathcal{H}_1 + \mathcal{H}_2$. This defines the case of weakly interacting subsystems, for which the total energy is

$$E = E_1 + E_2 . \quad (\text{III.2})$$

For a given choice of E_1 , the total energy E may be distributed among the two subsystems in $\Omega(E_1, E_2) = \Omega(E_1)\Omega(E_2)$ ways³² and the probability of finding the combined system in a state where subsystem 1 has an energy E_1 is proportional to this number, that is

$$P(E_1) \propto \Omega(E_1)\Omega(E - E_1) , \quad (\text{III.3})$$

where we have used Eq. III.2. Since the system is isolated, E is fixed, and the most likely value of E_1 is that maximizing the probability or, equivalently, its logarithm

$$\ln \Omega(E_1, E - E_1) = \ln \Omega(E_1) + \ln \Omega(E - E_1) . \quad (\text{III.4})$$

Thus, at equilibrium, E_1 will attain the value satisfying $\frac{\partial \ln \Omega(E_1, E - E_1)}{\partial E_1} = 0$. The use of this condition in Eq. III.4 and the introduction of the notation

$$\beta(N, V, E) \equiv \left(\frac{\partial \ln \Omega(N, V, E)}{\partial E} \right)_{N, V} \quad (\text{III.5})$$

yields

$$\beta(N_1, V_1, E_1) = \beta(N_2, V_2, E_2) . \quad (\text{III.6})$$

[†]For an ideal, monoatomic gas described by classical mechanics, $\Omega(N, V, E) \propto V^N E^{3N/2}$.³²

If we initially put all energy into subsystem 1, energy would be transferred into subsystem 2 until Eq. III.6 is satisfied. Eq. III.6 therefore expresses the condition for thermal equilibrium, a condition that in thermodynamics is related to maximization of the system entropy, S . When Eq. III.6 is satisfied, $\ln \Omega(E_1, E - E_1)$ is at its maximum, and it is therefore natural to define the entropy as

$$S(N, V, E) = k_B \ln \Omega(N, V, E) , \quad (\text{III.7})$$

where k_B is Boltzmann's constant. Since thermal equilibrium implies the satisfaction of Eq. III.6, β is expected to be related to the temperature. The use of the thermodynamic definition of temperature, $1/T = \left(\frac{\partial S}{\partial E}\right)_{(N,V)}$, along with the definition of β yields

$$\beta = \frac{1}{k_B T} . \quad (\text{III.8})$$

In the chemical laboratory it is much more convenient to prepare a system at constant temperature than at constant energy. In MS it is therefore desirable to mimic the latter situation. To that end, consider the system shown in Figure III.B

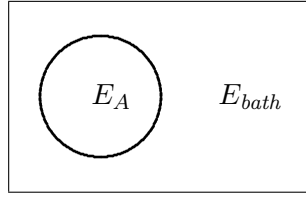


Figure III.B. A quantum mechanical system A weakly interacting with a heat bath.

Assume, that the quantum system A is prepared in one specific eigenstate $|i\rangle$ with an energy E_i determined from the time-independent Schrödinger equation

$$\mathcal{H}|i\rangle = (\mathcal{H}_A + \mathcal{H}_{bath} + \mathcal{H}_{int})|i\rangle = (E_i + \mathcal{H}_{int})|i\rangle \approx E_i|i\rangle \quad (\text{III.9})$$

by following arguments similar to those leading to Eq. III.2. The probability P_i of finding the system in state $|i\rangle$ will then be determined by the degeneracy of the bath $\Omega_{bath}(E - E_i)$ according to the postulate of equal a priori probabilities as

$$P_i = \frac{\Omega_{bath}(E - E_i)}{\sum_j \Omega_{bath}(E - E_j)} . \quad (\text{III.10})$$

Since $E - E_i = E_{bath} \gg E_i$ we may approximate $\ln \Omega_{bath}(E - E_i)$ by its Taylor expansion around $E_i = 0$ to first order

$$\ln \Omega_{bath}(E - E_i) \approx \ln \Omega_{bath}(E) - E_i \frac{\partial \ln \Omega_{bath}(E)}{\partial E} = \ln \Omega_{bath}(E) - \beta E_i , \quad (\text{III.11})$$

where the last equality has been obtained using the definition of β . Inserting in Eq. III.10 gives

$$P_i = \frac{e^{-\beta E_i}}{\sum_j e^{-\beta E_j}} \equiv Q^{-1} e^{-\beta E_i} , \quad (\text{III.12})$$

by which we define the partition function Q . Now we can calculate the ensemble average energy of the system A

$$\begin{aligned}\langle E \rangle_T &= \sum_i E_i P_i = Q^{-1} \sum_i E_i e^{-\beta E_i} \\ &= -\frac{\partial \ln Q}{\partial \beta} = -\frac{\partial k_B \ln Q}{\partial 1/T}.\end{aligned}\quad (\text{III.13})$$

By comparing to the thermodynamic relationship between the energy and the Helmholtz free energy (A), $E = \frac{\partial A/T}{\partial 1/T}$ we find that

$$A = -k_B T \ln Q. \quad (\text{III.14})$$

In general, the average value of an observable B is given as

$$\langle B \rangle = \frac{\sum_i e^{-\beta E_i} \langle i | B | i \rangle}{\sum_i e^{-\beta E_i}}. \quad (\text{III.15})$$

This expression need be transformed into its classical counterpart, in order to be useful in the application of the classical simulation methods. This is done by discretization of the classical coordinate and momenta variable space, the *phase space*, and observing that the Heisenberg uncertainty principle puts an upper bound on the granularity of this discrete representation.³² Here, merely the result is quoted^{8,31}

$$\langle B \rangle = \frac{\int d\mathbf{r}^N d\mathbf{p}^N e^{-\beta \mathcal{H}(\mathbf{r}^N, \mathbf{p}^N)} B(\mathbf{r}^N, \mathbf{p}^N)}{\int d\mathbf{r}^N d\mathbf{p}^N e^{-\beta \mathcal{H}(\mathbf{r}^N, \mathbf{p}^N)}}, \quad (\text{III.16})$$

where summation over states is turned into phase space integration over the coordinates \mathbf{r} and momenta \mathbf{p} of the N particles and $\mathcal{H}(\mathbf{r}^N, \mathbf{p}^N)$ is the classical Hamiltonian function. This is the ensemble average as obtained in the *canonical ensemble* (constant N , V , and T).

III.2 Molecular dynamics simulation

When conducting a chemical experiment it is common practice to prepare a sample of the system subjected to investigation and subsequently measure certain properties of the sample by collecting data for a period of time. A molecular dynamics (MD) simulation is in many respects equivalent to the chemical experiment. The model system, which we will here assume to be atomistic, is prepared in a reasonable configuration, the particles are given initial velocities and the system is then propagated according to the equations of motion³³

$$\begin{aligned}\dot{\mathbf{r}}_i(t) &= \mathbf{v}_i(t) \\ \dot{\mathbf{v}}_i(t) &= \mathbf{a}_i(t) = \mathbf{f}_i(t)/m_i = -\nabla_i U/m_i,\end{aligned}\quad (\text{III.17})$$

where \mathbf{r}_i , \mathbf{v}_i , and \mathbf{a}_i is the position, velocity, and acceleration of particle i , with mass m_i , \mathbf{f}_i the total force exerted on it by the other particles of the system, and U a potential model, as discussed in Chapter II. During the propagation, the desired quantities are sampled and their statistical accuracy can be improved by extending the propagation time.

Eq. III.17 is a system of $6N$ coupled first-order differential equations and is as such a standard numerical problem usually solved by finite difference schemes.³⁴ However, since the purpose of an MD simulation is to predict averages rather than computing an accurate trajectory, the most suitable integrator is not a general purpose algorithm. By far, the most time consuming task in an MD simulation is the calculation of the forces and it is therefore desirable that the integrator is able to use long time steps, still yielding good energy conservation. The time-reversibility of Newton's equations is also a property which should be reflected in the integrator. In general, energy conservation can be improved by shortening the time step which in turn increases the computational effort. Algorithms that show good compromise between accuracy and economy in terms of computational requirements are the Verlet^{8,35} class of integrators, here exemplified by the velocity form³⁶

$$\mathbf{r}(t + \Delta t) = \mathbf{r}(t) + \mathbf{v}(t)\Delta t + \frac{1}{2}\mathbf{a}(t)\Delta t^2 \quad (\text{III.18})$$

$$\mathbf{v}(t + \Delta t) = \mathbf{v}(t) + \frac{1}{2}[\mathbf{a}(t + \Delta t) + \mathbf{a}(t)]\Delta t. \quad (\text{III.19})$$

If the velocity is eliminated from Eq. III.18, the original coordinate form of the Verlet algorithm is found³⁵

$$\mathbf{r}(t + \Delta t) = 2\mathbf{r}(t) - \mathbf{r}(t - \Delta t) + \mathbf{a}(t)\Delta t^2 \quad (\text{III.20})$$

which can be derived by adding the Taylor expansions for $\mathbf{r}(t + \Delta t)$ and $\mathbf{r}(t - \Delta t)$. Time reversibility of this scheme is evident from the symmetric role of $\mathbf{r}(t + \Delta t)$ and $\mathbf{r}(t - \Delta t)$ in Eq. III.20.

The usefulness in a statistical mechanical sense of a time averaged property relies on the *ergodic hypothesis*. This states that time averaging and ensemble averaging are equivalent, i.e.

$$\bar{B} = \langle B \rangle \quad (\text{III.21})$$

where

$$\bar{B} = \lim_{t \rightarrow \infty} \frac{1}{t} \int_0^t dt' B(t'). \quad (\text{III.22})$$

This hypothesis will be justified in the following. Note that in Eq. III.22 it is implicitly assumed that \bar{B} is independent of the initial conditions $\Gamma(0) \equiv \{\mathbf{r}^N(0), \mathbf{p}^N(0)\}$. Therefore, the time average will not change if we choose to average also over initial conditions as

$$\bar{B} = \frac{1}{N_{ic}} \sum_i^{N_{ic}} \left[\lim_{t \rightarrow \infty} \frac{1}{t} \int_0^t dt' B(\Gamma(0)_i, t') \right]. \quad (\text{III.23})$$

In the limit of considering every possible initial state $N_{ic} \rightarrow \Omega(N, V, E)$ we obtain (disregarding a constant factor³¹)

$$\begin{aligned} \bar{B} &= \frac{1}{\Omega(N, V, E)} \int d\mathbf{r}^N d\mathbf{p}^N \delta(H - E) \left[\lim_{t \rightarrow \infty} \frac{1}{t} \int_0^t dt' B(\Gamma(0), t') \right] \\ &= \lim_{t \rightarrow \infty} \frac{1}{t} \int_0^t dt' \langle B(\Gamma(0), t') \rangle_{NVE}, \end{aligned} \quad (\text{III.24})$$

where the Kronecker δ assures that the integration is only over the part of phase space with energy E . The second equality is established by interchanging the order of integration and subsequently recognizing the phase space integral over constant E as the micro-canonical (constant N , V , and E) ensemble average. Due to the determinism of mechanics there is complete equivalence between averaging over the set of initial phase space points and the time-evolved ones; $\langle B(\Gamma(0), t') \rangle_{NVE}$ is independent of t' and

$$\bar{B} = \langle B \rangle_{NVE} . \quad (\text{III.25})$$

It is important to realize that even though a system is ergodic in principle there may be several reasons for it not to be ergodic in practice. This is the case for systems where large energetic barriers separate important portions of the configuration space as will be discussed in Chapter IV.

III.3 Monte Carlo simulation

A Monte Carlo (MC) simulation is conceptually very different from an MD simulation. Where the latter propagates the molecular system according to Newton's equations of motion and relies on ergodicity to provide ensemble averages from time averages, an MC simulation establishes the ensemble averages in a more direct fashion, as will be outlined in the following.

The goal is to compute ensemble averages

$$\langle B \rangle = \frac{\int d\mathbf{r}^N e^{-\beta U(\mathbf{r}^N)} B(\mathbf{r}^N)}{\int d\mathbf{r}^N e^{-\beta U(\mathbf{r}^N)}} \equiv Z^{-1} \int d\mathbf{r}^N e^{-\beta U(\mathbf{r}^N)} B(\mathbf{r}^N) \quad (\text{III.26})$$

now focusing on the most difficult configurational part of Eq. III.16.[†] Here Z is the configurational part of the partition function. Eq. III.26 gives the ensemble average of the property B as a probability weighted integration $\langle B \rangle = \int d\mathbf{r}^N \rho(\mathbf{r}^N) B(\mathbf{r}^N)$ where

$$\rho(\mathbf{r}^N) = \frac{e^{-\beta U(\mathbf{r}^N)}}{Z} \quad (\text{III.27})$$

is the probability density. The calculation of the denominator Z using traditional quadrature is of course exceedingly cumbersome primarily due to the dimensionality of the problem. However, the Metropolis scheme³⁷ allows for the generation of points in configuration space distributed according to $\rho(\mathbf{r}^N)$, requiring knowledge only of the potential energy $U(\mathbf{r}^N)$. Suppose we start at the point $\mathbf{r}^N = o$ in configuration space. From o we generate a *random* new configuration $\mathbf{r}^{N'} = n$ and denote the probability of going from o to n by $\pi(o \rightarrow n)$. If this probability can be determined from knowledge only of the configurations o and n , the successive chain of configurations will constitute a Markov chain. Since these configurations are drawn from the probability distribution $\rho(\mathbf{r}^N)$, they may be viewed as constituents of the ensemble. Thus, the desired ensemble averages can be calculated as we propagate along the Markov chain.

[†]If the property B is independent of \mathbf{p}^N the kinetic part of Eq. III.16 can be evaluated analytically, since classically $e^{-\beta \mathcal{H}(\mathbf{r}^N, \mathbf{p}^N)} = e^{-\beta K(\mathbf{p}^N)} e^{-\beta U(\mathbf{r}^N)}$ and the kinetic energy function $\mathcal{K}(\mathbf{p}^N)$ is merely a $3N$ dimensional Gaussian.

We proceed by evaluating the transition probability. This must obey the condition, that once an equilibrium distribution is established, it must not be destroyed. Therefore, the distribution must satisfy a steady state condition, which can be formulated as

... in a very large number of MC simulations on the same system the number of transitions into state o must equal the number of transitions leaving state o

or

$$\rho(o) \sum_{n \neq o} \pi(o \rightarrow n) = \sum_{n \neq o} \rho(n) \pi(n \rightarrow o) . \quad (\text{III.28})$$

This condition is most certainly fulfilled if each term on the left hand side equals the corresponding term on the right hand side, i.e. if

$$\rho(o) \pi(o \rightarrow n) = \rho(n) \pi(n \rightarrow o) , \quad \forall n , \quad (\text{III.29})$$

which is known as the condition of detailed balance. As already implicitly assumed, the procedure of going to state n from state o consists of two steps; selecting state n as a *trial configuration* [with probability $\alpha(o \rightarrow n)$] and subsequently accepting state n [with probability $\text{acc}(o \rightarrow n)$]. The outcome of both steps must be successful for the transition to occur so

$$\pi(o \rightarrow n) = \alpha(o \rightarrow n) \text{acc}(o \rightarrow n) . \quad (\text{III.30})$$

In a conventional MC simulation³⁷ α is chosen to be symmetric $\alpha(o \rightarrow n) = \alpha(n \rightarrow o)$, and with this choice the use of Eq. III.30 in Eq. III.29 yields

$$\frac{\text{acc}(o \rightarrow n)}{\text{acc}(n \rightarrow o)} = \frac{\rho(n)}{\rho(o)} = e^{-\beta[U(n)-U(o)]} , \quad (\text{III.31})$$

where the last equality follows from Eq. III.27. This condition is trivially satisfied by the choice

$$\text{acc}(o \rightarrow n) = \begin{cases} \frac{\rho(n)}{\rho(o)} & , \quad \rho(n) < \rho(o) \\ 1 & , \quad \rho(n) \geq \rho(o) \end{cases} , \quad (\text{III.32})$$

which yields for the transition probability

$$\begin{aligned} \pi(o \rightarrow n) &= \begin{cases} \alpha(o \rightarrow n) e^{-\beta[U(n)-U(o)]} & , \quad U(n) > U(o) \\ \alpha(o \rightarrow n) & , \quad U(n) \leq U(o) \end{cases} , \\ \pi(o \rightarrow o) &= 1 - \sum_{n \neq o} \pi(o \rightarrow n) . \end{aligned}$$

The MC algorithm consists of three steps which in a simulation undergo repetition

1. Select trial configuration n from current configuration o .
2. Generate a random number $\sigma \in [0; 1]$. Accept new configuration and replace o by n if and only if $\sigma < e^{-\beta[U(n)-U(o)]}$.
3. Compute averages.

Before this algorithm can be implemented it is necessary to elaborate on the procedure by which the trial configuration is selected; the trial move. The only restriction on α is that it must be symmetric which leaves considerable flexibility in the choice of trial moves. One very common choice is accomplished by selecting $\mathbf{r}^{N'} = n$ from $\mathbf{r}^N = o$ such that

$$\mathbf{r}^{N'} = \{\mathbf{r}'_1, \dots, \mathbf{r}'_i, \dots, \mathbf{r}'_N\} = \{\mathbf{r}_1, \dots, \mathbf{r}_i + \mathbf{\Delta}, \dots, \mathbf{r}_N\} , \quad (\text{III.33})$$

where i is picked at random, and $\mathbf{\Delta}$ has components $\Delta_\alpha = \delta(1 - 2\sigma_\alpha)$, where σ_α are random numbers satisfying $0 \leq \sigma_\alpha \leq 1$.

III.4 Long-range interactions

The simulation of a macroscopic sample with a number of particles on the order of Avogadro's number, is of course not possible. When simulating a liquid, it is thus necessary to impose some set of boundary conditions on the system in order to mimic bulk behavior. The goal is to reduce, and ideally remove, the influence of surface effects on the simulated properties. This is most conveniently done by introducing periodic boundary conditions and using either the minimum image convention in which each particle interacts with the nearest periodic image of all other particles or a spherical cut-off. In the latter approach each particle interacts with the nearest periodic image of all other particles within a sphere of radius r_c .

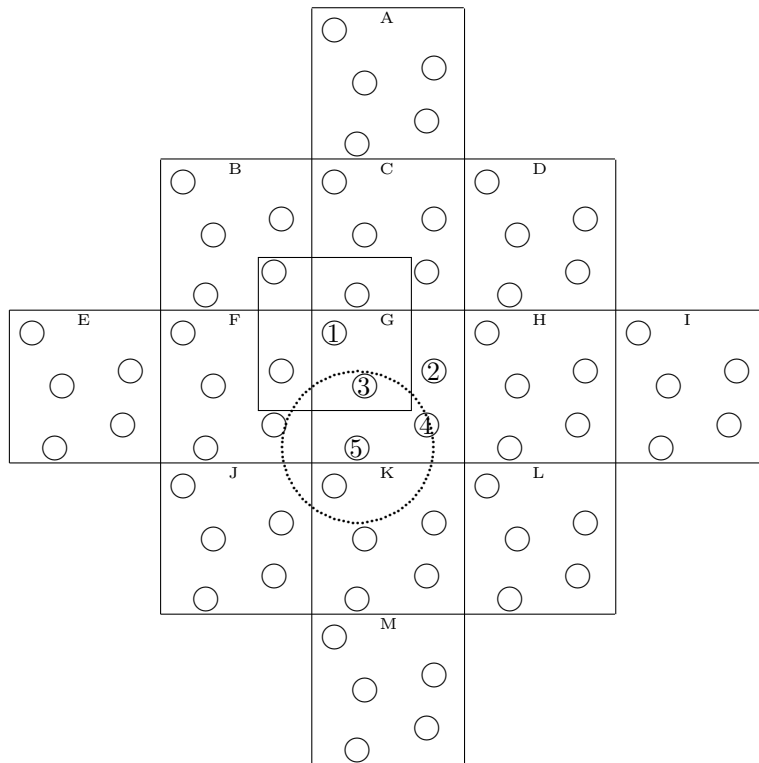


Figure III.C. Periodic boundary conditions in two dimensions. The simulation box G containing five particles is replicated in the x and y directions. The minimum image convention and spherical cutoff are demonstrated by the box centered on particle 1 and the dotted circle centered on particle 5, respectively.

This is illustrated in Figure III.C. If the minimum image convention is applied for particle 1, it interacts with the periodic image of particles: 4 in box B, 5 in box C, 2 in box F, and 3 in box G. If a spherical cut-off is used for particle 5 it will interact with the image of particles 3 and 4 in box G and that of particle 1 in box K, but not with any image of particle 2.

In the spherical cut-off treatment of an atomistic liquid the amount of neglected pair potential energy is proportional to $\int_{r_c}^{\infty} r^2 u_{pair}(r) dr$ if the density is considered to be uniform for $r > r_c$. For pair potentials u_{pair} with an asymptotic behavior as r^{-n} this integral diverges if $n \leq 3$. Interactions with this behavior, among which we find the very important cases of the Coulomb ($n = 1$) and dipole-dipole ($n = 3$) interactions, are commonly referred to as long-range. The most straightforward way to overcome this problem, would simply be to replicate the simulation box and compute the pair interaction energy as a so-called lattice sum

$$U_{lattice} = \frac{1}{2} \sum_{|\mathbf{m}| \leq m_{cut}} \sum'_{i,j} U_{ij}(\mathbf{r}_{ij} + \mathbf{m}L) , \quad (\text{III.34})$$

where L is the simulation box length, \mathbf{m} is a vector of integers, and the prime indicates that the $i = j$ term should be omitted for $\mathbf{m} = 0$. The integer m_{cut} should be increased until $U_{lattice}$ satisfies some criterion of convergence. The two-dimensional case is illustrated in Figure III.C; for $m_{cut} = 2$ the particles in box G should interact with all images in boxes A through M except their own image in box G. The direct summation in Eq. III.34 is extremely demanding in terms of computer resources. However, an efficient scheme for computing the sum was developed by Ewald³⁸ which was later generalized to dipole interactions.³⁹ The original expression by Ewald is valid in the case of the infinitely replicated system surrounded by a conductor, whereas Eq. III.34 holds when the total system is surrounded by vacuum. The connection between the two schemes was established by deLeeuw *et al.*⁴⁰ by the introduction of the so-called surface term.^{8,31} Recently, faster schemes, such as the particle-mesh Ewald summation⁴¹ have been developed.

An alternative to the Ewald summation (ES) also in widespread use is the reaction field (RF) method in which the interactions are truncated spherically as when simulating under spherical cut-off conditions. But instead of assuming that the droplet of radius r_c is surrounded by vacuum, the medium beyond the cut-off is treated as a homogeneous and isotropic dielectric extending to infinity. The dipole moment of the sphere induces a polarization in the surrounding dielectric, causing a *reaction field* that interacts with the dipole at the center of the sphere.^{8,42,43} The magnitude of the reaction field is found by solving Laplace's equation for the potential inside and outside the cavity.⁴³ It is given as

$$R_{i,\alpha} = \frac{2(\epsilon_{RF} - 1)}{(2\epsilon_{RF} + 1)r_c^3} M_{i,\alpha} , \quad (\text{III.35})$$

where ϵ_{RF} is the dielectric constant of the surrounding medium and $M_{i,\alpha}$ the α -component of the total dipole moment of the sphere with radius r_c centered on particle i . The ES and RF methods are described in detail in Paper VI, where they are generalized to polarizable systems.

III.5 Molecular simulation on parallel computers

The application of MS to the large systems of interest in biochemical science and industry poses great computational demands. Systems containing tens of thousands of atoms and millions of pair-interactions must be propagated for several million simulation steps, preferably in not more than a few days. Modern state-of-the-art computers are parallel, and, in order to be used efficiently, need parallel programs. Also those with no access to such facilities, can benefit from parallel computing, since the low cost of PC hardware has motivated the construction of parallel architectures by interconnecting a large number of PC's or workstations to form so-called Beowulf systems. These are capable of providing nearly super-computer CPU power at a very low price.

Parallel computers are often categorized by how the system memory is accessed and are as such either of the shared memory or distributed memory type. Shared memory machines have a number of processors connected to a global memory bank through which they can communicate. In distributed memory machines each processor is connected to its own memory, and data must be transferred explicitly by means of a fast inter-connector. Shared memory computers are fairly easy to program; much of the work is done by the compiler through directives supplied by the programmer but the design works well only on systems with a small number of processors. Distributed memory machines can utilize hundreds of processors, the price, unfortunately, is paid by the programmer who has to explicitly program the parallelism.

To facilitate easy programming of different parallel computers and the writing of portable programs, sets of useful routines for a distributed memory environment, such as routines to send data to a particular processor, have been standardized. One such standard, MPI,^{44, 45} has been implemented on a very large number of platforms - including shared memory computers. By conforming to the MPI interface, code can be produced requiring nothing but a recompilation in order to function on architectures as different as SGI Origin 2000 shared memory machines and a group of PC's connected by a fast switch.

In connection with the work presented in Paper VII the MOLSIM program⁶ was parallelized using the MPI interface. The parallelization was targeted at efficiency for the systems investigated in that work; polarizable systems on the order of a few thousand atoms. When conducting MD simulations of polarizable systems, the bulk of the computational load is spent evaluating the electric potential, field, the electric field-gradient and, in turn, the induced dipole moments and intermolecular forces - see Section VI.1 and Paper VII for details. For efficiency, MOLSIM employs a neighbor list^{8, 35} in conjunction with a spherical cut-off. Each entry in the neighbor list represents a pair of molecules, and the list holds at least all interacting pairs of molecules. Energy and forces are evaluated by looping through all entries in the neighbor list, computing the contributions from the pairs within the spherical cut-off. The parallelization was realized by making each processor responsible for computing contributions from a particular portion of the neighbor list. The parallel algorithm consists - in a simplified version - of six steps:

1. Each processor computes the neighbor list, if necessary.
2. Processor P : compute contribution to potential, field, or field-gradient from pair inter-

actions in the P 'th part of the neighbor list.

3. Gather: Processor 1 receives contributions to potential, field, or field-gradient from processors $2, \dots, n_{proc}$ and performs a summation of the contributions.
4. Broadcast: Processor 1 sends the summed result to processors $2, \dots, n_{proc}$.
5. Each processor computes energy and forces on all particles, and propagates the particles.
6. Processor 1: Produce output and compute averages, if necessary.

It is only in step 2 that the processors perform different tasks. In step 1 and 5 the processors perform identical operations which is more efficient than computing partial results and subsequently invoking additional communication. In the actual implementation, step 3–4 are combined in a single MPI functionality. The trajectory is known to each processor so only a single processor is involved in producing output and computing averages in step 6.

When the ES is invoked in the simulation of a polarizable system, the potential, field, and field-gradient all consist of both real-space and reciprocal-space contributions.^{VI} The real-space contributions are evaluated as pair interactions, and are thus readily parallelized according to the procedure described above, but a different approach is required for the reciprocal-space contributions. As indicated by Eqs. II.13–II.15 contributions to the electrostatic potential, field, and field-gradient at atom i are all derivatives of the reciprocal-space energy contribution with respect to a property of atom i and have the general form^{VI}

$$\mathcal{F}_i = \sum_{\mathbf{k} \neq 0} m(i, \mathbf{k}) \sum_j \mathcal{Q}(j, \mathbf{k}) , \quad (\text{III.36})$$

where $m(i, \mathbf{k})$ depends on properties of atom i (e.g. its charge, dipole moment, and position) and the \mathbf{k} -vector. In the parallel implementation, the atoms are distributed among the n_{proc} processors. Each processor, P , is responsible for the calculation of \mathcal{F}_i , $i \in P$, hence the scheme

1. Processor P : Calculate $\mathcal{Q}_P(\mathbf{k}) = \sum_{j \in P} \mathcal{Q}(j, \mathbf{k})$ for every value of \mathbf{k} .
2. Gather and broadcast of $\mathcal{Q}_P(\mathbf{k})$ - each processor now holds the sum over j in Eq. (III.36) for each \mathbf{k} .
3. All processors: Compute the final sum over \mathbf{k} .

A certain amount of overhead is, however, involved since factors $e^{i\mathbf{k} \cdot \mathbf{r}_i}$ enter both $m(i, \mathbf{k})$ and $\mathcal{Q}(i, \mathbf{k})$ ^{VI} and thus have to be evaluated in both the first and last step. For the purpose of serial computation it is therefore more efficient to maintain another algorithm in which the $e^{i\mathbf{k} \cdot \mathbf{r}_i}$ factors are evaluated only once.

IV Chemical reactions in solution

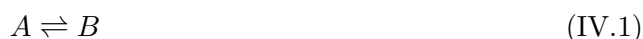
Since the bulk of applied chemistry occurs in solution, it is highly desirable to understand in detail how the solvent influences the reacting system. The role of the solvent in this respect is many-sided. It will alter the potential energy surface upon which the reaction takes place, e.g. through stabilization of polar or ionic species by a polar solvent. It will act as both an energy source and an energy sink, typically as the former when the reaction barrier is ascended and as the latter when the reaction barrier is descended. It will also directly influence the dynamics of the reaction by enhancing or impeding the motion of the reaction complex.

For a chemical reaction to be tractable by classical molecular dynamics simulation, non-adiabatic coupling, tunneling, and other quantum phenomena must be unimportant. The potential energy surface must account for the breaking and formation of bonds, deeming a global quantum mechanical description of the reaction system necessary in its construction. Given a suitable potential for the reaction system and solvent, the investigation of the reaction may be pursued by initiating trajectories in the reactant channel and following their path to the product channel. Unfortunately, this simple approach is not feasible since a chemical reaction, on the time scale normally considered by MD simulations, is a very rare event. That is, the majority of these trajectories will remain in the reactant region for a very long time. However, should unlikely fluctuations bring the system to the *transition state*, through which the reaction is assumed to proceed, the reaction will occur quickly. To that end, it is the formation of the transition state that is a rare event.

The solution to this problem is provided by non-equilibrium statistical mechanics. This formulation allows the reaction rate to be determined as the product of the probability of finding the reaction system at the transition state and the rate by which the transition state configuration is decomposed.^{46,47} The former factor is an equilibrium property which can be calculated by MS methods; all dynamics of the reaction enter via the decomposition rate. And since the reaction occurs readily once the transition state is reached, the decomposition rate is also available from MD simulation.

IV.1 Reaction rate constants described by non-equilibrium statistical mechanics

In this Section, a brief presentation of non-equilibrium statistical mechanics applied to chemical kinetics, based on that by Chandler,^{46,47} is given. Consider the isomerization reaction



described by the phenomenological rate equations

$$\begin{aligned}\frac{dc_A}{dt} &= -k_{A \rightarrow B}c_A(t) + k_{B \rightarrow A}c_B(t) \\ \frac{dc_B}{dt} &= k_{A \rightarrow B}c_A(t) - k_{B \rightarrow A}c_B(t),\end{aligned}\quad (\text{IV.2})$$

where c_A , c_B , $k_{A \rightarrow B}$, and $k_{B \rightarrow A}$ are the concentrations of A and B and the rate constants for the forward and backward reaction, respectively. For a closed system, the sum of these rates is zero, and at equilibrium $\dot{c}_A = \dot{c}_B = 0$, implying

$$\frac{k_{A \rightarrow B}}{k_{B \rightarrow A}} = \frac{\langle c_B \rangle}{\langle c_A \rangle} \equiv K, \quad (\text{IV.3})$$

by which the equilibrium constant K is defined. Suppose the equilibrium is perturbed at time zero by increasing the concentration of A by Δc_A , such that $c_A(t) = \langle c_A \rangle + \Delta c_A(t)$ and $c_B(t) = \langle c_B \rangle - \Delta c_A(t)$. Inserting these expressions in Eq. IV.2 and the use of Eq. IV.3 allows the rate of decay of the perturbation to be determined as

$$\frac{d\Delta c_A(t)}{dt} = -(k_{A \rightarrow B} + k_{B \rightarrow A}) \Delta c_A(t) \quad (\text{IV.4})$$

with the solution

$$\Delta c_A(t) = \Delta c_A(0)e^{-(k_{A \rightarrow B} + k_{B \rightarrow A})t} \equiv \Delta c_A(0)e^{-t/\tau_R}, \quad (\text{IV.5})$$

which defines the reaction time constant τ_R .

We proceed by considering the microscopic perspective in the framework of linear response theory. The idea is to apply a perturbation at $t = -\infty$ which will shift the equilibrium concentrations. At $t = 0$ the perturbation is instantaneously turned off, allowing us to monitor the decay of the system toward equilibrium. We imagine that the progression of the reaction can be described by a *reaction coordinate* s , for which the reactant state A , product state B , and the transition state are characterized by $s < 0$, $s > 0$, and $s = 0$, respectively. The microscopic analogy of increasing the concentration of A is to add to the Hamiltonian \mathcal{H}_0 a term favoring A , i.e. states with $s < 0$, as

$$\mathcal{H} = \mathcal{H}_0 - \lambda\theta(-s), \quad (\text{IV.6})$$

where λ is a parameter measuring the strength of the perturbation and $\theta(t)$ is the Heaviside step function, $\theta(t) = 1$ for $t > 0$ and $\theta(t) = 0$ otherwise. For convenience, we will define $\theta_A \equiv \theta(-s)$ and $\theta_B \equiv \theta(s)$. The connection to the macroscopic formulation is now established by observing that

$$\Delta c_A = \langle c_A \rangle_\lambda - \langle c_A \rangle = \langle \theta_A \rangle_\lambda - \langle \theta_A \rangle, \quad (\text{IV.7})$$

where subscript λ indicates ensemble averaging in presence of the external perturbation. The change in concentration is characterized by the *static response* of the concentration to the perturbation, i.e.

$$\frac{\partial \Delta c_A}{\partial \lambda} = \frac{\partial \langle \theta_A \rangle_\lambda}{\partial \lambda} = \frac{\partial}{\partial \lambda} \frac{\int d\Gamma e^{-\beta(\mathcal{H}_0 - \lambda\theta_A)} \theta_A}{\int d\Gamma e^{-\beta(\mathcal{H}_0 - \lambda\theta_A)}}, \quad (\text{IV.8})$$

where we use the shorthand notation Γ for all coordinates and momenta introduced in Section III.2. Differentiation yields

$$\left(\frac{\partial \Delta c_A}{\partial \lambda}\right)_{\lambda=0} = \beta \langle \theta_A \rangle (1 - \langle \theta_A \rangle) = \beta \langle c_A \rangle \langle c_B \rangle, \quad (\text{IV.9})$$

so to first order in λ

$$\Delta c_A = \beta \lambda \langle c_A \rangle \langle c_B \rangle. \quad (\text{IV.10})$$

Consider now the situation when the perturbation is removed at $t = 0$. Since the perturbation was applied at $t = -\infty$, the non-equilibrium distribution experienced now in the absence of the perturbation, is the equilibrium distribution when the perturbation is turned on. Therefore, the time evolution of Δc_A for $0 < t \ll \tau_R$ is given as

$$\Delta c_A(t) = \langle \Delta \theta_A(t) \rangle_\lambda = \frac{\int d\Gamma e^{-\beta(\mathcal{H}_0 - \lambda \theta_A)} \Delta \theta_A(t)}{\int d\Gamma e^{-\beta(\mathcal{H}_0 - \lambda \theta_A)}}, \quad (\text{IV.11})$$

where $\Delta \theta_A(t) = \theta_A(t) - \langle \theta_A \rangle$. The time evolution of $\theta_A(t)$ should be governed by the unperturbed Hamiltonian \mathcal{H}_0 since the perturbation was turned off at $t = 0$. By expanding $e^{-\beta(\mathcal{H}_0 - \lambda \theta_A)}$ as a Taylor series around $\lambda = 0$ and considering terms to first order in λ only yields

$$\Delta c_A(t) = \beta \lambda \langle \Delta \theta_A(0) \Delta \theta_A(t) \rangle = \beta \lambda \left(\langle \theta_A(0) \theta_A(t) \rangle - \langle \theta_A \rangle^2 \right), \quad (\text{IV.12})$$

where we have used that $\langle \Delta \theta_A \rangle = 0$. Elimination of λ by the use of Eq. IV.10 gives

$$\Delta c_A(t) = \Delta c_A(0) \frac{\langle \theta_A(0) \theta_A(t) \rangle - \langle \theta_A \rangle^2}{\langle c_A \rangle \langle c_B \rangle}. \quad (\text{IV.13})$$

By comparing to the macroscopic result, Eq. IV.5, it is evident that

$$e^{-t/\tau_R} = \frac{\langle \theta_A(0) \theta_A(t) \rangle - \langle \theta_A \rangle^2}{\langle c_A \rangle \langle c_B \rangle}. \quad (\text{IV.14})$$

However, at times so short that the system is still in the transition state region this equation is not expected to hold, since the right hand side definitely will not decay exponentially according to τ_R . Only for times long compared to the barrier crossing time, will the equation hold. By taking the time-derivative of Eq. IV.14 we obtain

$$-\tau_R^{-1} e^{-t/\tau_R} = \frac{\langle \theta_A(0) \dot{\theta}_A(t) \rangle}{\langle c_A \rangle \langle c_B \rangle} = -\frac{\langle \dot{\theta}_A(0) \theta_A(t) \rangle}{\langle c_A \rangle \langle c_B \rangle}. \quad (\text{IV.15})$$

For times longer than the barrier crossing time, but much shorter than τ_R , $e^{-t/\tau_R} \approx 1$. The use of Eq. IV.3 and $\langle c_A \rangle + \langle c_B \rangle = 1$ gives $\tau_R^{-1} = k_{A \rightarrow B} / \langle c_B \rangle$ and inserting this result in Eq. IV.15 yields

$$k_{A \rightarrow B} = \frac{\langle \dot{\theta}_A(0) \theta_A(t) \rangle}{\langle c_A \rangle}, \quad (\text{IV.16})$$

where the numerator may be elaborated on noting that

$$\dot{\theta}_A = \dot{\theta}(-s) = \dot{s} \frac{\partial \theta(-s)}{\partial s} = -\dot{s} \delta(s). \quad (\text{IV.17})$$

Inserting in Eq. IV.16 yields

$$k_{A \rightarrow B}(t) = \frac{\langle -\dot{s}(0)\delta[s(0)]\theta_A(t) \rangle}{\langle c_A \rangle} = \frac{\langle \dot{s}(0)\delta[s(0)]\theta_B(t) \rangle}{\langle \theta_A \rangle}, \quad (\text{IV.18})$$

where the last equality follows from $\langle \dot{s}(0)\delta[s(0)] \rangle = 0$. Since $\lim_{t \rightarrow 0^+} \theta[s(t)] = \theta(\dot{s})$, we may obtain the initial rate constant as

$$k_{A \rightarrow B}(0) = \frac{\langle \dot{s}(0)\delta[s(0)]\theta(\dot{s}) \rangle}{\langle \theta_A \rangle}. \quad (\text{IV.19})$$

The property averaged in the numerator of Eq. IV.18 can be characterized as the *reactive flux* crossing the transition state, where *reactive* means that the trajectory ultimately ends in the product region as determined by the factor $\theta_B(t)$. In Eq. IV.19 all trajectories initially directed toward the product region are considered reactive. This is equivalent to the assumption in transition state theory of no recrossing of the barrier,[†] and Eq. IV.19 is indeed equivalent to the rate constant obtained from transition state theory. Recrossings will, as discussed above, occur on a time scale much faster than τ_R , causing $k_{A \rightarrow B}(t)$ to display an initial fast decay followed by a plateau, determining the phenomenological rate constant. Assuming the plateau is reached after Δt , the observed rate constant is given as $k_{A \rightarrow B}(\Delta t)$. To that end, we may define the transmission factor as

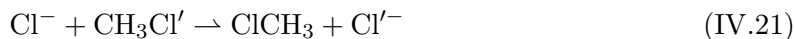
$$\langle \eta \rangle = \frac{k(\Delta t)}{k(0)}, \quad (\text{IV.20})$$

where the subscript on the rate constant has been omitted. The transmission factor can be calculated as the fraction of trajectories initiated at the transition state leading to reaction,^{49,50} and combined with the transition state theory result to yield the exact rate constant.

IV.2 Simulation of an S_N2 reaction in aqueous micro-solution

The nucleophilic, bimolecular substitution (S_N2) reaction mechanism and its uni-molecular counterpart S_N1 are among the most studied in chemistry. Comparative studies of S_N2 reactions in gas-phase and in liquid phase have revealed reaction rates differing by several orders of magnitude,⁵¹ and theoretical investigations of S_N2 reactions have dealt with accounting for these differences.

The subject of Paper I is the S_N2 reaction



occurring in clusters of water molecules. The chemical reaction was described by a complete potential energy surface for the $[\text{ClCH}_3\text{Cl}]^-$ system including the C-H motion,⁵² and a flexible, polarizable model was used for the water molecules. Chemical rate constants were calculated as a function of cluster size and temperature using the dynamical model of Eq. IV.20.

[†]The original paper of Eyring⁴⁸ does in fact discuss the possibility of recrossing, taken into account in his rate equations by a transmission factor.

Moreover, MD simulations were carried out to investigate the structure and dynamics of the reaction clusters.

The rate constant and reaction barrier as functions of the number of solvent molecules was found to follow a rather irregular pattern from the gas-phase values to the values for the reaction in bulk aqueous solution. This irregularity was found to be related to the enhanced stabilization of the ion-dipole reactant complex at certain cluster sizes. MD simulations showed that the chloride ion of the reactant complex as in aqueous solution is able to coordinate a large number of water molecules, whereas the chlorine atoms in the transition state complex coordinate a lower number of water molecules in their first solvation shell. This causes a stronger stabilization of the reactant complex compared to that of the transition state complex. Further, the water clusters were found to be weaker coordinated to Cl^- than in the liquid state related to the lack of acceptors for the kinetic energy gained by these water molecules in close proximity of the chloride ion.

IV.3 An entire reaction coordinate method

The model utilized in Paper I provides information only about a very limited part of reaction coordinate space. Essentially only two points are considered, the reactant state and the transition state. Although knowledge of these two configurations is sufficient to obtain the reaction rate constant, it is of substantial interest to probe the entire reaction coordinate space. As discussed above, direct simulation will fail to establish adequate sampling of the transition region, but this may be remedied by so-called umbrella sampling.⁵³ In this technique an additional artificial potential term, referred to as an umbrella potential, is introduced by which the reaction coordinate is restricted to a particular interval. The reaction coordinate space is thus split into discrete intervals, and an umbrella sampling simulation is performed on each interval. Subsequently, the combined effort of these simulations provide the full probability distribution or potential of mean-force (PMF) along the reaction coordinate. However, it is difficult to decide, *a priori*, the form of the umbrella potential.

An improved procedure has been suggested by Engkvist and Karlström.⁵⁴ They introduce a modified MC procedure, in which an umbrella potential is constructed as the simulation progresses. Thus, the entire reaction coordinate (ERC) space is sampled during a single simulation. Consider the one-dimensional probability distribution of the reaction coordinate s , which can be calculated from the probability density in the canonical ensemble, Eq. III.26, as

$$P(s) = \int d\mathbf{r}^N \delta(s' - s) \rho(\mathbf{r}^N) = \frac{\int d\mathbf{r}^N \delta(s' - s) e^{-\beta U(\mathbf{r}^N)}}{\int d\mathbf{r}^N e^{-\beta U(\mathbf{r}^N)}}. \quad (\text{IV.22})$$

If an umbrella potential $U'(s)$ depending solely on the reaction coordinate is added to the potential energy, a different probability distribution is obtained as

$$P'(s) = \frac{\int d\mathbf{r}^N \delta(s' - s) e^{-\beta[U(\mathbf{r}^N) + U'(s)]}}{\int d\mathbf{r}^N e^{-\beta[U(\mathbf{r}^N) + U'(s)]}}. \quad (\text{IV.23})$$

This new probability distribution can be expressed in terms of the original distribution up to

a normalization constant as

$$P'(s) = P(s)e^{-\beta U'(s)} . \quad (\text{IV.24})$$

The most effective sampling of the reaction coordinate space occurs when $P'(s)$ is uniform, i.e. when U' is chosen to be proportional to $\beta^{-1} \ln P(s)$. In that case U' efficiently cancels the PMF defined as

$$W(s) = W_0 - \beta^{-1} \ln P(s) , \quad (\text{IV.25})$$

where W_0 defines the arbitrary zero-point. However, from Eq. IV.25 we note that knowledge of $P(s)$ is required to calculate $W(s)$. Since $P(s)$ is the result of the simulation, this is not immediately a feasible approach. As mentioned, a solution is offered by modifying U' as the simulation advances ensuring that U' ultimately converges toward W . The modification procedure is constructed to force the MC algorithm to move away from the region populated at equilibrium, and thereby cause the ascending of reaction barriers. In a discrete representation of s , U' is updated as

$$U'(s_i)^{new} = U'(s_i)^{old} + \beta^{-1} \ln [1 + u(M)] , \quad \lim_{M \rightarrow \infty} u(M) = 0 , \quad (\text{IV.26})$$

where s_i is the current value of the reaction coordinate and the positive update function, $u(M)$, depends on the number of performed simulation steps, M . Unfortunately, this simulation procedure is not a valid MC simulation as described in Section III.3 since the potential is altered in each step violating the symmetry requirement on the α matrix (Eq. III.30). However, when the simulation potential *has* converged, the limit $u(M) = 0$ is reached, and α becomes symmetric. Thus, the subsequent part of the simulation satisfies the formal requirement for an MC simulation. Therefore, the number of simulation steps must be much larger than the number of steps required to converge U' .

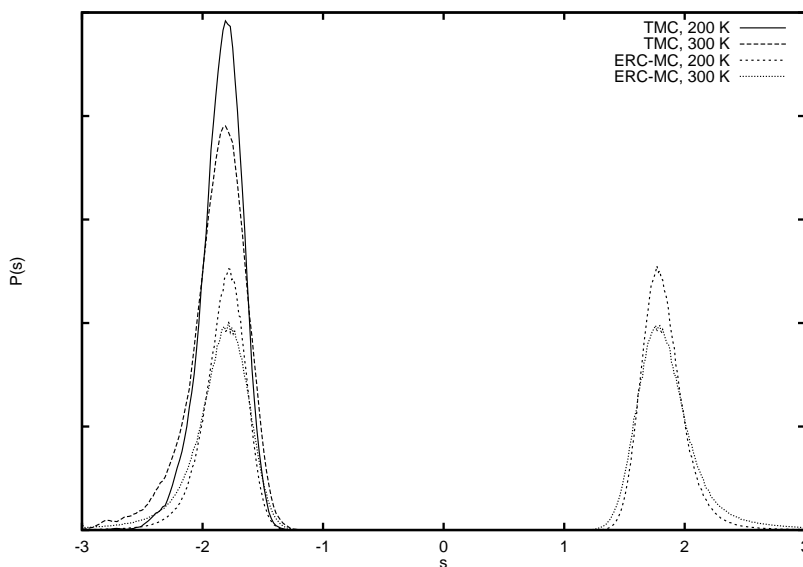


Figure IV.A. Gas-phase probability distribution for the reaction coordinate of the chloride-methylchloride reaction system obtained using both a traditional MC (TMC) simulation and an entire reaction coordinate MC (ERC-MC) simulation.

Figure IV.A shows the probability distribution $P(s)$ for the chloride-methyl-chloride reaction system in gas-phase at two different temperatures. The potential energy surface and the reaction coordinate used is the same as in Paper I; $s = r_{Cl_1C} - r_{Cl_2C}$. The form chosen for the update function in Eq. IV.26 was $u(M) = M^3 / \max_i \{e^{\beta U'(s_i)^{old}}\}$ and the number of steps used in each simulation $2 \cdot 10^7$. It is evident that the traditional MC simulation probes only the reactant region, whereas the ERC-MC method correctly determines the symmetric probability distribution. The maximum of $P(s)$ corresponds to the ion-dipole complex $Cl^- \cdots CH_3Cl$. The decreasing probability as $|s|$ is increased beyond the maximum shows that the breaking of this complex requires a substantial amount of energy, and therefore is unlikely.

Preliminary results from studying the same system in aqueous solution are also available. During the course of these solution studies, it became apparent that MC sampling of the solvent motion was inadequate to model the relatively rapid structural changes experienced by the water molecules close to the reaction complex. This was improved upon, *ad hoc*, by employing a combined ERC-MC/MD procedure allowing an MD description of the solvent.

Simulations were performed by immersing the chloride-methyl-chloride system in a cavity formed by removing water molecules from an equilibrated system of 64 molecules.[†] After equilibration the system was propagated for $1 \cdot 10^7$ combined steps consisting of two ERC-MC steps followed by a single MD step. The intramolecular potential described in Paper I was used in conjunction with the SPC water potential.⁵⁵

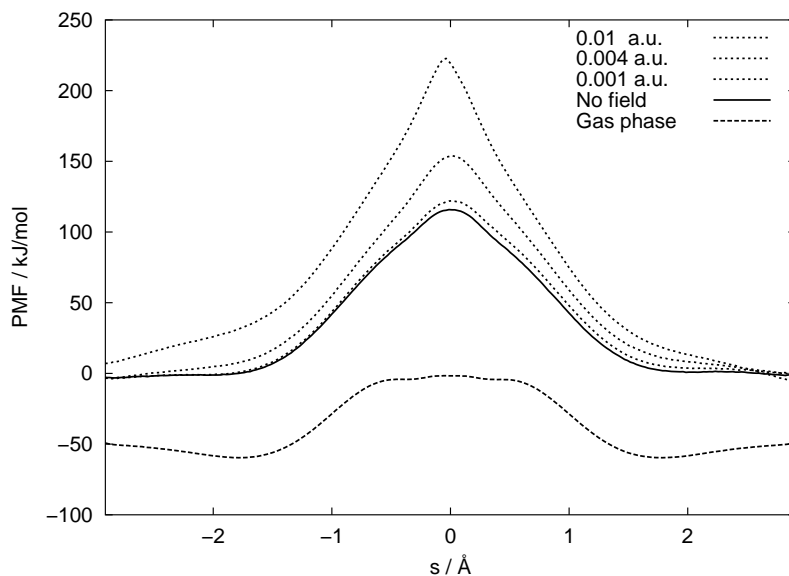


Figure IV.B. PMF for the chloride-methyl-chloride reaction system. Results are shown for the solvated system with an external electric field (dotted) of $E=0.01$, 0.004 , and 0.001 a.u. from top to bottom, no external field (full), and for the system in gas-phase (dashed).

The PMF for the reaction system in solution and in the gas-phase is shown in Figure IV.B. The weak bumps in the upper part of the barrier for the gas-phase PMF is an artifact of the

[†]This number of water molecules is generally much too low to account properly for the solvation.

applied potential energy surface. Ideally, the PMF in solution should reflect the symmetry of the reaction, and the deviations from reflection symmetry in s of the PMF is caused by inadequate statistical convergence. Upon solvation, the stabilization of the ionic reactant/product species is enhanced compared to that of the transition state complex. This causes the reaction barrier to increase from ~ 60 kJ/mol in the gas-phase to ~ 115 kJ/mol in solution. This is in good agreement with both the experimental result of 111 kJ/mol⁵⁶ and other theoretical estimates of 116⁵⁵ and 110 ± 2 kJ/mol⁵⁷ despite the low number of solvent molecules used in the present study. Apart from increasing the barrier height, the solvent also causes a dramatic change in the shape of the barrier. At about $|s| = 0.6$ Å the gas-phase barrier flattens appreciably, whereas the barrier in solution continues to increase as $|s|$ decreases, resulting from weaker solvent interaction due to lowering of the dipole moment of $[\text{ClCH}_3\text{Cl}]^-$ as $|s|$ tends to zero. The minimum for the ion-dipole complex in the gas-phase is absent in aqueous solution; the energetic cost of breaking the ion-dipole attraction, is compensated for in solution by stronger solvation of the separated chloride and methyl-chloride fragments.

The reaction system has also been studied under the influence of an external, static electric field $\mathbf{E}_{ex} = E_{ex}\hat{\mathbf{k}}$. Within the electric dipole approximation, the interaction energy is given as

$$U_{ex} = -\mathbf{M} \cdot \mathbf{E}_{ex} , \quad (\text{IV.27})$$

where $\mathbf{M} = \sum_i^N \boldsymbol{\mu}_i$, is the total dipole moment of the system and $\boldsymbol{\mu}_i$ is the dipole moment of particle i . The presence of an external field thus promotes the alignment of particle dipole moments in the $\hat{\mathbf{k}}$ direction. If the reaction system was fixed with $\hat{\mathbf{k}}$ parallel to the Cl^- -C-Cl axis, the chemical equilibrium would be controlled by the sign and magnitude of E_{ex} , a mechanism that has been studied for proton transfer reactions.⁵⁸

Figure IV.B also presents the PMF exhibited by the system in an external, static field at different field strengths. The field strengths should be compared to the internal field experienced by the molecules in a water simulation, discussed in Paper II and V, and in Section VI.1.1. The electric field experienced by the oxygen atom in a water simulation is ~ 0.05 a.u. In comparison, the strength of the fields applied here range from medium to very strong. The presence of an external field is observed to further enhance the barrier height by a few kJ/mol for the weakest field and by almost 100 kJ/mol for the strongest. This is caused by enhanced stabilization by the external field of the most dipolar conformation, i.e. the reactant system. However, disregarding convergence problems which are substantial for the strongest field, the symmetry of the PMF is maintained. Although the external field favors population of one particular channel, this does not prevent the ERC-MC procedure from ascending the, now larger, reaction barrier. Once the barrier is crossed, the positive interaction with the external field will cause the entire system to rotate, thereby switching the role of the reactant/product states.

The solvation as a function of reaction coordinate has also been investigated. Figure IV.C shows the number of water molecules in the first solvation shell of the Cl atoms as function of the reaction coordinate. A water molecule is regarded as a member of the first solvation shell of Cl if $r_{OCl} < 4$ Å as in Paper I.

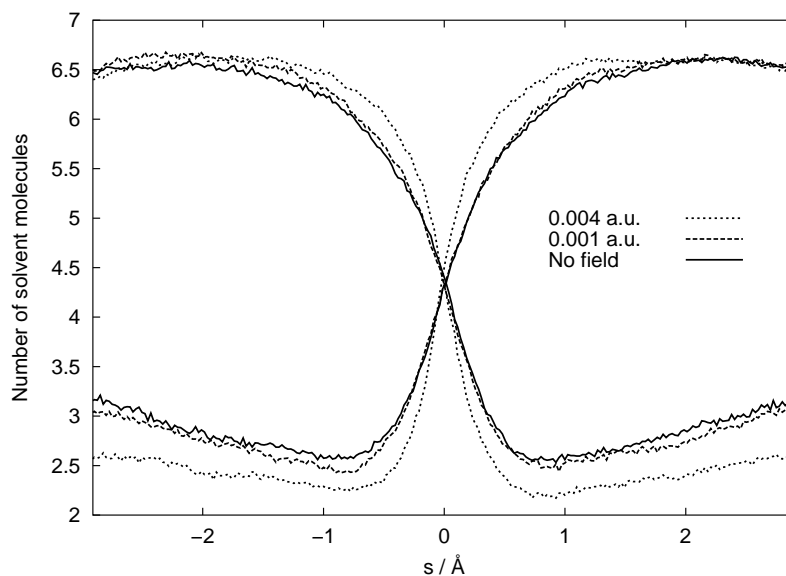


Figure IV.C. The number of water molecules in the first solvation shell of the two chlorine atoms as a function of the reaction coordinate s .

At the transition state, each Cl atom is coordinated to about 4.5 water molecules. As the reaction proceeds toward product or reactant channel, one Cl atom gains charge and separates from the methyl-chloride fragment, and is therefore able to coordinate a larger number of water molecules - about 6.5. The corresponding numbers found in Paper I were about 1.5 and 4 water molecules for the transition state and ion-dipole complex, respectively. The chlorine atom in CH_3Cl coordinates 3 water molecules when no external field is applied. When an external field of 0.001 a.u. is applied, the situation remains almost unchanged. However, when the field strength is increased to 0.004 a.u. the solvation is altered. The number of solvent molecules for Cl^- is increased by less than 0.5 for $|s| < \sim 1.5 \text{ \AA}$ and decreased by 0.5 for the covalently bonded chlorine. It thus appears that the solvation shell around ClCH_3 attains a less dense but more dipolar conformation when the external field is applied.

For a reaction such as Eq. IV.21 involving charged species, the most important role of a solvent is that of stabilizing these. This process will completely govern the gas-to-liquid shift of the rate constant for the reaction, as evident from the substantial deviation of the corresponding activation barriers of $\sim 50 \text{ kJ/mol}$. As such, the ERC method facilitates the study of such reactions by providing the effective reaction barriers, although it appears that the number of simulation steps required to achieve convergence is considerable. The ERC method should be particularly useful in multi-barrier systems, where conventional umbrella sampling becomes increasingly cumbersome.

V Properties of solvated molecules

The investigation of the changes in a molecule occurring upon solvation requires the introduction of a solvent model. This concept is a rather broad one but the models can nevertheless usually be characterized as of either microscopic or macroscopic nature. In a microscopic model, solvation is treated at the molecular level by incorporating the perturbation from the solvent into the quantum mechanical description of the molecular properties of the solute. Conversely, a macroscopic model provides macroscopic properties from *effective* solute molecular properties assumed to be given. In the present work, the focus has been on the microscopic modeling of solvation.

The attempts to include solvation in current, accurate *ab initio* methods can, more or less, be characterized as being either continuum, supermolecular, or semi-continuum approaches. In the continuum solvent models, the molecular monomer is envisioned as enclosed in a cavity of a linear, homogeneous and isotropic dielectric, and solvation is modeled by the polarization of this medium. This is to a large extent analogous to the reaction field method briefly described in Section III.4, which is a special case of the continuum model. In the supermolecular approach, solvation is modeled by the explicit inclusion of - at least - the first solvation shell in the *ab initio* calculation. The semi-continuum approach combines the continuum and supermolecular approaches by including solvent molecules explicitly and immersing the entire supermolecular system in a dielectric medium. In most continuum and semi-continuum studies, the cavity is chosen to be spherical and thus is described by its radius only. This reduces the number of considered parameters, but nevertheless cavity size effects must be considered in these models.⁵⁹

Although semi-continuum models in general perform well, all these three methods possess inherent problems or limitations. It has been established that pure continuum models fail to give a satisfying description of solvent effects since neither local, short-range interactions nor inhomogeneous environments such as hydrogen bonding are properly accounted for. The supermolecular model, on the contrary, does not account for long-range interactions, unless a very large number of solvent molecules are included. The semi-continuum models formally include both short- and long-range interactions, but it is still an inherent requirement, that a representative structure of the solvent shell included in the calculation can be established. Even when this criterion is met solvation is still considered from a static viewpoint and in doing so, it is difficult to account for the temperature-dependence of the liquid property of interest.

Attempts have been made to combine MS and supermolecular methods. Subsystems, con-

sisting of a molecule and its first solvation shell, have been generated from MD simulations and then subjected to supermolecular or semi-continuum calculations.^{60–62} This overcomes the requirement of a single representative solvent structure since the simulations can be performed at a particular temperature. In this way the temperature effect of the molecular property is explicitly accounted for. However, the large number of supermolecular or semi-continuum calculations required renders the method computationally very expensive. Moreover, the inclusion of concentration effects would require a tremendous amount of work since the generated subsystems would have to encompass all relevant dimer, trimer, etc. configurations.

V.1 A microscopic, perturbational solvent model

An alternative way to combine statistical mechanical simulations with *ab initio* quantum chemical calculations to model solvation is by the use of intermolecular perturbation theory (IPT). The work described in Papers II–V was devoted to exploring solvation effects on different molecular properties by invoking an IPT solvent model. The gas-to-liquid shift of a molecular property can be expanded as a perturbation series, which contains products of property derivatives with respect to the perturbation and the magnitude of the perturbation. The task of computing the gas-to-liquid shift of a molecular property according to the IPT method is thus separated into two parts:

- Quantum chemical calculations of molecular property derivatives for the unperturbed molecule. These properties have to be calculated *once* for each molecule. No concerns regarding the solvent enter this part of the calculation.
- Statistical mechanical simulations for calculating the ensemble average of the magnitude of the perturbation, e.g. electric field or geometry distortion. All properties of the solvent, temperature, concentration etc., is taken into account here but the results may then be used for the calculation of the solvent effects on *any* molecular property.

Consequently, concentration effects, which are very difficult (if not impossible) to handle in semi-continuum and supermolecular models, can also be determined, simply by performing the simulations at the concentration of interest. Further, since the two parts are independent, it is possible to increase the quality of either part separately.

Inherent to the IPT solvent model is the assumption that a given molecular property under the influence of a solvent, B_{liq} , may be expressed as a sum of the vacuum value and a solvation term

$$B_{liq} = B_{vac} + B_{sol} . \quad (\text{V.1})$$

This expression is merely a consequence of regarding solvation as a perturbation of the solute molecule. Since solvation is manifested via intermolecular interactions, according to Eq. II.1 the solvation term should be composed as

$$B_{sol} = B_{ele} + B_{disp} + B_{exch} . \quad (\text{V.2})$$

Since the electrostatic perturbation is caused by the polarization of the solute arising from the electric field and field-gradient impinging on it, the induction contribution must be included

in B_{ele} - see below. In addition, an indirect geometry distortion term will arise, since the molecular geometry of the solute is altered compared to the gas-phase geometry. At normal densities, exchange and overlap effects are expected to be small,^{63,64} and will not be treated here. Finally, when connection is made to a particular experiment, additional terms may arise. For example, when a chemical shift is measured, the magnetic field experienced by the solute molecule is modified by the anisotropy of the magnetizability of the solvent molecules.⁶⁵ This effect is corrected for by an additional term in the expression for the gas-to-liquid shift for nuclear magnetic shielding.¹¹

In polar liquids such as water, the electrostatic term is the most important. It may be expanded as^{66,67}

$$B_{ele} = B'_\alpha E_\alpha + \frac{1}{2} B''_{\alpha,\beta} E_\beta E_\alpha + \dots + \frac{1}{3} B'_{\alpha\beta} E_{\alpha\beta} + \frac{1}{6} B''_{\alpha\beta,\gamma\delta} E_{\gamma\delta} E_{\alpha\beta} + \dots, \quad (\text{V.3})$$

where E_α and $E_{\alpha\beta}$ defined by Eqs. II.17 and II.18 are components of the electric field and the electric field-gradient, respectively, arising from the presence of the solvent. B'_α and $B''_{\alpha,\beta}$ are derivatives of B with respect to the electric field and $B'_{\alpha\beta}$ and $B''_{\alpha\beta,\gamma\delta}$ are derivatives with respect to the electric field-gradient. Since these derivatives are monomer properties the ensemble average of the electrostatic contribution is

$$\langle B_{ele} \rangle = B'_\alpha \langle E_\alpha \rangle + \frac{1}{2} B''_{\alpha,\beta} \langle E_\beta E_\alpha \rangle + \frac{1}{3} B'_{\alpha\beta} \langle E_{\alpha\beta} \rangle, \quad (\text{V.4})$$

where Eq. V.3 has been truncated after the three most important terms. Induced electric moments in the solvent contribute to the electric field and field-gradient, thereby accounting for induction effects, as mentioned above. To obtain an accurate description of the electrostatic environment, the interaction potential utilized in the simulation must correctly describe the charge distribution of the molecule. This would not be the case for an empirical potential for which the charge-like parameters are provided by fitting to experimental properties. Such demands are better suited by the use of a potential model obtained from intermolecular perturbation theory such as NEMO.

So far, the issue of which centers to include in the expansion has not been addressed. Some properties, such as the nuclear shielding, which primarily depend on the local electronic structure around a particular nucleus calls for an atomic expansion. Hence, derivatives of the nuclear shielding tensor with respect to the electric field and the electric field-gradient should be carried out for the nucleus of interest in the solute molecule, and combined with fields and field-gradients at that nucleus obtained from MS. Other properties, such as the molecular polarizability, will depend upon the global electronic structure making it natural to allow the molecular polarizability to depend on the electrostatic environment of the entire molecule.

The term accounting for the dispersion interaction contribution to the solvent effect is given as

$$\langle B_{disp} \rangle = \frac{1}{2} \sum_i B'''_{\alpha,\beta} \langle E_0^2 \rangle_{\alpha\beta}^i, \quad (\text{V.5})$$

where an atomic expansion has been adopted. The fluctuation potential $\langle E_0^2 \rangle_{\alpha\beta}^i$ is assessable from molecular simulation and is closely related to the dispersion energy,⁶⁸ Eq. II.24

$$U_{disp} = -\frac{1}{4} \sum_i \alpha_{i,\alpha\beta} \langle E_0^2 \rangle_{\alpha\beta}^i . \quad (\text{V.6})$$

For the NEMO potential,²⁶ the fluctuation potential may be approximated as

$$\langle E_0^2 \rangle_{\alpha\beta}^i = \sqrt{C} \frac{\bar{\omega}^A \bar{\omega}^B}{\bar{\omega}^A + \bar{\omega}^B} \sum_j \alpha_{j,\gamma\delta} T_{ij}^{\alpha\gamma} T_{ij}^{\beta\delta} , \quad (\text{V.7})$$

where $\alpha_{j,\alpha\beta}$ is a component of the polarizability tensor on atom j ,⁶⁹ $T_{ij}^{\alpha\gamma}$ is defined in Eq. II.12, and $\bar{\omega}^A$ is the average ionization potential introduced in Eq. II.24. C is a scaling factor for the local polarizabilities^{II} of 1.89 calibrated to the $\text{H}_2 - \text{H}_2$ system.⁷⁰

V.1.1 Molecular property derivatives

The property derivatives, entering Eqs. V.3 and V.5, can be computed by quantum chemical methods as properties of the solute molecule in vacuum. The solvent effects considered by the present model arise from the inertial or nuclear degrees of freedom in the liquid, and it is thus the static response of the solute molecule that need be addressed.

Ideally, the derivatives in Eqs. V.3 and V.5 would be calculated by response theory in quantum chemical programs. In practice, finite difference methods could be applied. In the latter case the molecular property of interest is calculated in the presence of a uniform external electric field or field-gradient. By calculating the property at different magnitudes of the field, first- and higher-order derivatives can be computed. This method has for example been used to calculate nuclear shielding derivatives.⁷¹

Finite difference methods do, however, become inadequate when it is desirable to calculate the simultaneous dependence of a molecular property on field and field-gradient at different nuclei. In that case we have employed a *point charge method*. Analogously to Eq. V.1 the property B calculated for a molecule interacting with a set of point charges, i , is given as the sum of the molecular property in vacuum and a difference term, arising from the presence of the charges

$$B^i = B_{vac} + \Delta B^i . \quad (\text{V.8})$$

If assumed that the electrostatic interactions alone are responsible for the difference, then, in analogy with Eq. V.4, for a single configuration we may expand ΔB^i as

$$\Delta B^i = B'_\alpha E_\alpha^i + \frac{1}{2} B''_{\alpha,\beta} E_\beta^i E_\alpha^i + B'_{\alpha\beta} E_{\alpha\beta}^i . \quad (\text{V.9})$$

The electric field E_α^i and field-gradient $E_{\alpha\beta}^i$ arising from the set of charges i are readily available from Eqs. II.17 and II.18. Since ΔB^i can be obtained from quantum chemical calculations in which the point charges i are explicitly included, the derivatives B'_α , $B''_{\alpha,\beta}$, and $B'_{\alpha\beta}$ can be obtained from least squares fitting to the set $\{\Delta B^i, E_\alpha^i, E_{\alpha\beta}^i\}$. That is, the derivatives are determined as to reproduce the computed set of values ΔB^i . This point charge method has been employed in other contexts.^{72–75}

V.2 Chemical shifts of liquid water

Nuclear Magnetic Resonance (NMR) techniques are among the most important to the investigation of structure and dynamics of chemical compounds. NMR is extensively used in the study of biomolecules, in which it is widely used to characterize hydrogen-bonding. These studies have revealed that the gas-to-liquid shift of the donor hydrogen chemical shielding is strongly correlated to the strength of the hydrogen bond.⁷⁶ To that end, an understanding of the origin of these shifts is desirable. Nuclear magnetic resonance parameters have also been extensively studied in quantum chemistry.⁷⁷

In Papers II and III the temperature dependent gas-to-liquid chemical shifts of water were examined using the IPT approach described above. In Paper II the chemical shift was modeled by electrostatic and dispersion contributions according to Eqs. V.3 and V.5, the electrostatic contribution, however, was truncated after the linear and quadratic field terms. The electric field ensemble averages and distributions were obtained from MD simulation using a polarizable NEMO potential,³⁰ whereas shielding polarizabilities and hyperpolarizabilities of Rizzo *et al.*⁷¹ were used. The distributions of non-vanishing electric field components were found to be almost completely described by Gaussian functions. All contributions to the gas-to-liquid shift were found to decrease with increasing temperature. The model was able to reproduce both the experimental chemical shift and its temperature-dependence for hydrogen, but neither for oxygen. Further, the effect arising from the distortion of the molecular geometry upon solvation was estimated by calculating the gas-phase chemical shift at two experimental molecular geometries of liquid water. The effect was found to be substantial for oxygen (-10 and -5 ppm) but modest for hydrogen (-1.4 and -0.7 ppm).

In Paper III the model was improved by extending the electrostatic contributions to include the linear field-gradient term of Eq. V.3. To calculate the required quadrupole shielding polarizabilities the point charge method described in Section V.1.1 was employed. Shielding polarizabilities, hyperpolarizabilities, and quadrupole shielding polarizabilities were calculated at both the Hartree-Fock (HF) and Complete Active Space Self-Consistent Field (CASSCF) levels of theory. MD simulations using the same potential as in Paper II provided ensemble averages and distributions of the non-vanishing electric field-gradient components. The linear field-gradient contribution was found to be substantial for oxygen (-9.7 ppm) and its inclusion improved the correspondence with experiment both with respect to magnitude and temperature-dependence. For hydrogen the contribution was small, -0.7 ppm, leaving the proton shift in good agreement with experiment.

In summary, IPT performs well for the proton shift, whereas the modeling of the oxygen shift is substantially more problematic. In the work of Buckingham and Tantirungrotechai^{75, 78} a very similar approach is applied to nuclear magnetic shielding changes in HF upon the formation of $\text{Ar} \cdots \text{HF}$ and $\text{HF} \cdots \text{CO}_2$, and compared to results from supermolecular calculations on the complexes. In accordance with our findings, they conclude that their model provides a very good description of the proton shift, whereas the results for F are much less encouraging. It is therefore evident that more work must be done to address these difficulties, the origin of which, at present, is unclear.

V.3 The geometry of the water molecule in liquid water

It is thought-provoking, that many of the most popular rigid potential models applied for liquid water use the gas- or solid-phase geometry although their purpose is the modeling of liquid water. Moreover, in the framework of the present IPT solvent model it is interesting to estimate the liquid phase geometry, and thereby assess the indirect geometry distortion contribution mentioned in Section V.1 in a more consistent manner.

Paper IV describes an investigation of the temperature dependent gas-to-liquid shift of the molecular geometry of water by means of the IPT method. The solvent effect on the molecular gradient and Hessian was assumed to depend on the electrostatic and van der Waals interactions with the solvent. Since these properties were considered in the normal-coordinate representation, all gradient and Hessian components were allowed to depend on the electrostatic environment of all three atoms. Gradient and Hessian derivatives with respect to the electric field and field-gradient were thus obtained using the point charge method at both the HF and CASSCF level. Equipped with the molecular gradient and Hessian of the solvated water molecule we used a single Newton-Raphson optimization step

$$\mathbf{x} = \mathbf{x}_{vac} - (\mathbf{H}_{vac} + \mathbf{H}_{sol})^{-1} \mathbf{g}_{sol} \quad (\text{V.10})$$

to obtain the estimated liquid phase molecular geometry \mathbf{x} . Here, \mathbf{H}_{sol} is the solvent shift of the molecular Hessian relative to the gas-phase Hessian \mathbf{H}_{vac} . The molecular gradient was assumed to be zero in the gas-phase causing the liquid phase gradient to consist of only the solvent shift \mathbf{g}_{sol} . The gas-to-liquid shift ($\Delta r_{OH} \approx 1$ pm and $\Delta \alpha \approx 2^\circ$) was found to be of similar accuracy as both other theoretical and experimental estimates.

Since the potential energy surface in Eq. V.10 is expanded around the gas-phase geometry no direct calculation of the normal modes in the liquid phase was possible. However, the solvent effect on the vibrational frequencies was estimated from the available data and were found to be in reasonable agreement with experimental results.

V.4 The refractive index of liquid water

The frequency-dependent refractive index of a material to a large extent determines its potential use in the fabrication of fiber-optics. An understanding on a microscopic basis of refractivity would greatly facilitate the development of such devices.

Paper V presents the results from employing different solvent models in calculating the refractive index of liquid water. The IPT method was used to calculate the dynamic polarizability of the water molecule in the liquid phase as a function of temperature and frequency. The gas-to-liquid shift of the molecular polarizability was assumed to be caused solely by electrostatic and van der Waals interactions at all three atomic sites, and it was therefore assumed that the molecular polarizability can be represented by a sum of atomic contributions. This has been shown to be an appropriate assumption.^{69,79,80} Due to the atomic distributed model, we calculated the necessary polarizability derivatives by the point charge method at both the HF and CASSCF level for different basis sets.

Polarizabilities for the solvated water molecule were also obtained from more conventional microscopic solvent models; the supermolecular and semi-continuum approaches, the latter

utilizing the recent Iterative Self-Consistent Reaction Field (ISCRF) method.⁸¹ Refractivities $n(\omega)$ were subsequently[†] calculated using two different macroscopic models; either as

$$n(\omega) = \sqrt{1 + 4\pi N\alpha(\omega)} , \quad (\text{V.11})$$

where N is the number density of the liquid and $\alpha(\omega)$ the effective, average molecular polarizability at frequency ω , or by the Lorentz-Lorenz⁸² model

$$n(\omega) = \sqrt{\frac{3 + 8\pi N\alpha(\omega)}{3 - 4\pi N\alpha(\omega)}} . \quad (\text{V.12})$$

Comparisons were also made to simpler models, in which correlated gas-phase polarizabilities were used in Eqs. V.11 and V.12, complying to the conventional use of these equations.^{43, 83}

In general it was found that the use of gas-phase polarizabilities in conjunction with Eq. V.12 worked surprisingly well in explaining both the dispersion and the temperature-dependence of the refractive index. Eq. V.12 is, however, well known to exaggerate the optical polarization of the continuous medium present in its derivation.^{43, 83} It was found necessary to account for electron correlation in the quantum chemical point charge calculations required by the IPT model. However, for strongly perturbing point charge configurations at the CASSCF level, the absorption edge was observed to move into the frequency range under consideration which in turn lead to an artificially high dispersion. The IPT model was found to give an improved description of the temperature-dependence of n_D as compared to the use of Eq. V.11 with gas-phase polarizabilities, making it evident that the temperature-dependence of the refractivity cannot be explained solely by the temperature dependence of the number density.

V.5 Summary

The abilities of the IPT microscopic solvent model have been tested for different properties. Bearing in mind the computational efficiency of the model, its performance has been satisfactory. Especially the modeling of the gas-to-liquid proton shift has been successful. The solvent effect of this property was found to be governed by the electrostatic contribution, a contribution dominated by the linear field term. In the light of these results, it should be prosperous to extend the study of proton shifts to other liquids and solutions.

The nuclear magnetic shielding may be regarded as a 'local' property depending mostly on the electron distribution around a particular nucleus. On the other hand, the molecular gradient, Hessian, and polarizability are 'true' molecular properties, depending on the entire electron distribution of the molecule. The gas-to-liquid shift of the latter properties will therefore depend on solvent interactions occurring throughout the molecule, whereas for the nuclear shielding it is reasonable to consider only interactions at the nucleus of interest. In the IPT model we have chosen the atomic positions as a representative set of interaction sites

[†]The ISCRF method uses Eq. V.12 to establish self-consistency between $\alpha(\omega)$ and $n(\omega)$. By requiring the experimental $n_D = n(589\text{nm})$ reproduced by the model the cavity radius is eliminated as a free parameter. See Paper V for details.

for the former properties, thereby establishing a need for the point charge method. But it may be argued that this set of centers be extended to include e.g. bond centers. In any case the procedure of determining field- and field-gradient derivatives is cumbersome by the use of the point charge method. As any fitting procedure operating with a modest number of parameters, dependencies among these are likely to interfere. Moreover, in order to give a proper determination of the second-order field derivatives (hyperpolarizabilities), a substantial field strength must be applied, but conversely, care must be taken of not perturbing the molecule too strongly, as experienced in Paper V. Analytical derivatives are therefore highly desirable, but currently not available, since the anisotropic electric fields and field-gradients experienced in liquids must be taken into account.

VI Applications to liquid properties

VI.1 Long-range interactions in polarizable liquid water

The problem of long-range interactions in MS has drawn much attention. It is well established that to model even qualitatively the dielectric properties of polar liquids, long-range interactions must be addressed. Further, free energies of solvation are also sensitive towards the correct treatment of long-range interactions.

In Paper VI the ES and RF methods described in Section III.4 were generalized to a system possessing polarizabilities in addition to atomic charges and dipole moments. The induced dipoles are determined by a minimization of the total interaction energy with respect to the induced dipole moment $\{\mu_{i,\alpha}^{ind}\}$ according to response theory.⁸⁴ The result is

$$\mu_{i,\alpha}^{ind} = \alpha_{i,\alpha\beta} E_{i,\beta}^{tot}, \quad (\text{VI.1})$$

where $E_{i,\alpha}^{tot}$ is the α -component of the electrostatic field on atom i arising from charges, permanent, and induced dipole moments of atoms in other molecules

$$E_{i,\alpha}^{tot} = \sum_{j \neq i} T_{ij}^{\alpha} q_j + T_{ij}^{\alpha\beta} (\mu_{j,\beta}^{ind} + \mu_{j,\beta}^{perm}). \quad (\text{VI.2})$$

Since $\mu_{i,\alpha}^{ind}$ enters the right hand side of this equation, the induced dipole moments must be determined by iterating Eqs. VI.1 and VI.2 to self-consistency. The induction energy is given as

$$U_{ind} = -\frac{1}{2} \sum_i \mu_{i,\alpha}^{ind} E_{i,\alpha} = -\frac{1}{2} \sum_i \alpha_{i,\alpha\beta} E_{i,\alpha} E_{i,\beta}^{tot}, \quad (\text{VI.3})$$

where $E_{i,\alpha}$ is the α -component of the electrostatic field at atom i arising from charges and permanent dipoles only and Eq. VI.1 has been used to arrive at the last equality. When this expression is compared to Eq. II.22 it is noted to contain additional terms. These have their origin in higher-order perturbation terms.⁸⁵

The procedure in a numerical application for calculating the electrostatic and induction part of the energy, forces, and virial consists of the following steps (details are given in Paper VI).

1. Calculate the electrostatic potential (required to calculate the energy) and field from charges and permanent dipole moments.
2. Calculate induced dipole moments by self-consistent iteration (or by prediction⁸⁶).

3. Calculate electrostatic and induction energies.
4. If induced dipole moments were predicted, calculate electric field from induced dipole moments.
5. Calculate electrostatic field-gradient (required to calculate the forces).
6. Calculate forces.
7. Calculate virial.

When long-range interactions are included in the simulation the expressions for the interaction energy, electrostatic potential, field, field-gradient, force, and virial are all changed, i.e. modifications occur in all steps of the algorithm above. Paper VI gives these expressions for both ES and RF conditions along with numerical results facilitating the implementation of these methods for polarizable molecules.

In Paper VII the theoretical results of Paper VI have been implemented in the MOLSIM program⁶ and subsequently utilized to simulate liquid water under ES and RF conditions using the polarizable NEMO potential.³⁰ The paper presents various structural, dynamic, and dielectric properties obtained from trajectories of several ns. The results have been compared with those obtained by a simple spherical cut-off and using the unpolarizable SPC/E potential model.¹⁰ It was found that the use of the simple spherical cut-off tends to exaggerate the polarization of the system, in turn leading to an overestimated interaction energy, a sharper liquid structure, and slower dynamics compared to ES and RF methods. Further, the RF method was found to exhibit a more substantial system size sensitivity as compared to ES.

VI.1.1 The effect of boundary conditions on electric field and field-gradient

In connection to the IPT solvent model presented in Chapter V it is interesting to examine the effect of including long-range interactions in the simulations providing the electric field and field-gradient, entering Eq. V.4. Table VI.A quotes the electric field calculated for a spherical cutoff (SC), RF, and ES conditions for systems composed of 64, 216, and 512 water molecules. The results were obtained from simulations (a)–(h) in Paper VII except for the smallest system and SC conditions which were obtained from a recent 3 ns simulation.

Table VI.A. Total electric field in liquid water at different boundary conditions and system sizes. Units are 10^{-3} a.u. Error estimates are calculated by averaging over 20 ps blocks.

System size	64	216	512	64	216	512
	Oxygen			Hydrogen		
SC ^a	49.45(8)	48.66(7)	-	53.03(4)	52.29(4)	-
RF	45.38(4)	46.08(2)	46.58(2)	48.96(3)	49.84(2)	50.37(2)
RF _e	-	46.17(2)	-	-	49.94(1)	-
ES	46.71(7)	46.76(3)	46.79(3)	50.49(4)	50.53(2)	50.59(2)

First of all, the effects are modest which is not surprising, considering the results for the induced dipole moment reported in Table III of Paper VII. The differences for a system of

216 water molecules are within 6%. For both oxygen and hydrogen, SC yields the highest values for the field and the RF method the lowest.

When the system size effects are examined it is striking that ES gives the same result for oxygen, considering error bars, for all three system sizes. For hydrogen only the smallest and largest systems differ, the difference is however less than 0.2%. The RF results display a substantial system size dependence. As the system size increases, the RF results approach the ES result, but even for the largest system the deviation between RF and ES is larger than the deviation between ES(512) and ES(64). System size effects appears to be even larger for SC although difficult to assess from only two points. Also SC appears to approach ES as the system size is increased.

The effect of changing ϵ_{RF} of the dielectric medium entering the RF model (Eq. III.35), has also been considered. Table VI.A (results denoted RFe) shows that if ϵ_{RF} is changed to the experimental value the results for the field are brought closer to those obtained by ES, but the effect reduces the difference between RF(216) and ES(216) by less than 20%.

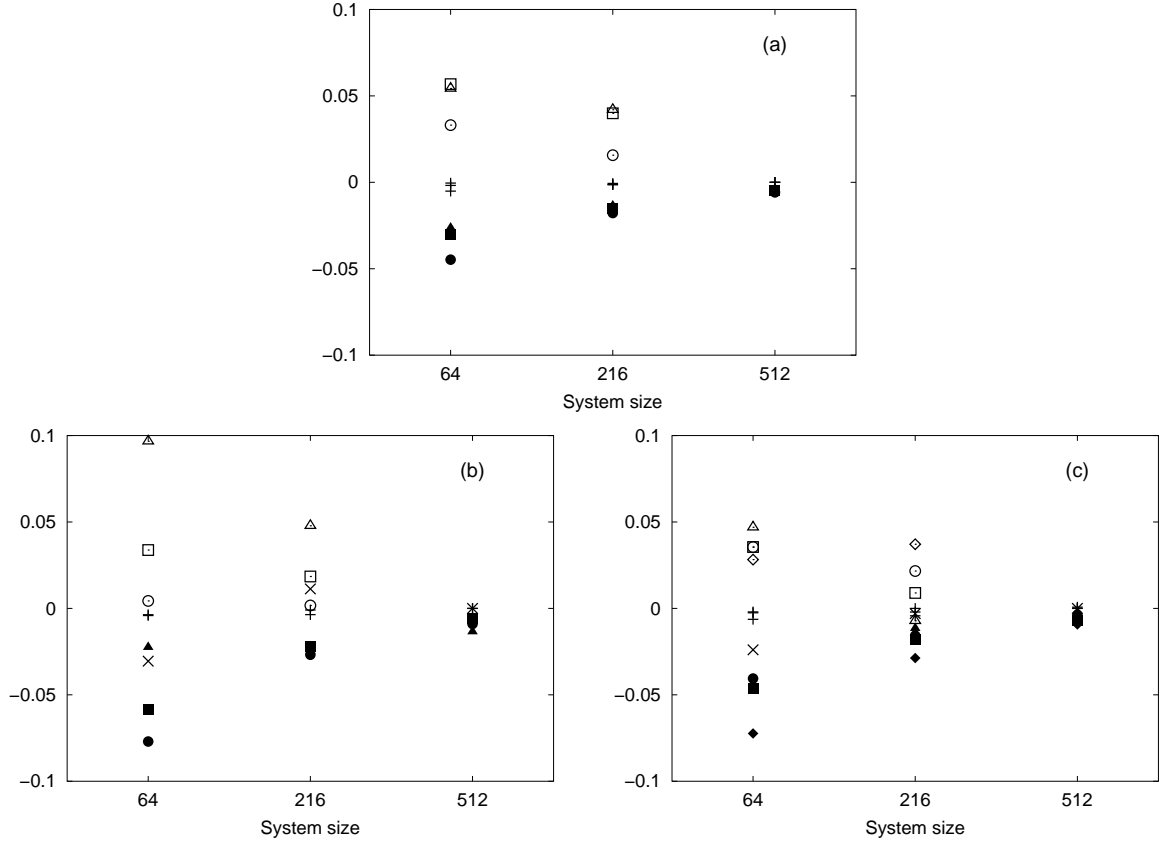


Figure VI.A. Relative errors in (a) the electric field components, (b) the electric field-gradient on oxygen, and (c) the electric field-gradient on hydrogen. Results are shown for SC (open symbols), RF (filled symbols), and ES (+), except for E_{zz} designated (\times). The designations of the different components are as follows. (Square): $E_{O,z}$, E_{xx} , (circle): $E_{H,x}$, E_{yy} , (triangle): $E_{H,z}$, E_{zz} , and (diamond): $E_{H,xz}$.

These trends are clarified in Figure VI.A in which relative errors compared to the ES results

for the largest system of the non-vanishing Cartesian components of the electric field and field-gradient are displayed. The relative error is thus defined as

$$\Delta = \frac{E - E_{ES(512)}}{E_{ES(512)}}. \quad (\text{VI.4})$$

The relative errors are also small for the field-gradient, although somewhat larger for the field-gradient components on oxygen. For the medium sized system all errors are within $\pm 5\%$. As noted above the ES errors are very small - all below 1% except the zz field-gradient component. This component is in error by about -3% for both oxygen and hydrogen in the smallest system, and slightly overestimated for oxygen in the medium sized system.

For SC, the field and field-gradient components are systematically overestimated. However, it is striking that the $E_{O,yy}$ component almost reproduces the ES result, whereas $E_{O,zz}$ is in error by 10% for the smallest system. This could be related to the qualitative differences observed in the dielectric properties of SC and ES. For the RF method all components are underestimated but the errors are reduced when the system size is increased. Moreover, the error reduction is more pronounced and systematic than for SC. Further, in contrast to the SC results the errors for the different components at a given system size are almost the same, the exception being $E_{H,xz}$ for which the error is slightly larger than for the other hydrogen field-gradient components. For the largest system all RF errors are below 2%.

In summary, the ES procedure is preferred in the calculation of electrostatic properties. Even for the smallest system ES performs surprisingly well. The RF method underestimates all field and field-gradient components, but the errors are fairly constant and are substantially reduced when the system is increased. For SC the field and field-gradient components are generally overestimated. The SC errors are larger than for the RF method, display a large variation, and their reduction upon increasing system size is less significant than for the RF method. From a computational perspective, the electrostatic properties of water should thus be calculated from an ES simulation for a system of 64 water molecules. In doing so, the accuracy of the properties is slightly improved compared to a medium sized system using SC or RF conditions and the computational effort is reduced by a factor of three.^{VII}

VI.2 A comparative study of effective and polarizable potentials.

Paper VIII describes a comparative, temperature dependent study of a polarizable NEMO potential³⁰ and an effective two-body potential derived from that. The motivation of the study was to improve the understanding of the connection between explicitly polarizable potentials and two-body potentials, which represent polarization in an average or effective sense, as discussed in Section II.1. This study was undertaken using water as a test case. In the polarizable NEMO potential, the electrostatics are represented by atomic charges, dipole moments, and anisotropic polarizabilities. A parameterized potential is obtained from this by replacing the permanent dipole moment on atom i , μ_i^{perm} by $\mu_i^{perm} + \lambda \langle \mu_i^{ind} \rangle$. Here $\langle \mu_i^{ind} \rangle$ is the average induced dipole moment obtained from a simulation using the explicitly polarizable potential and λ a scalar, temperature dependent parameter. The effective

potential is obtained at $\lambda = \lambda^*$, the value of which was determined by conducting several simulations for different values of λ . This procedure ensures that the effective potential bears the strongest possible resemblance to the polarizable potential. The value of λ^* was determined such that the effective potential as far as possible yields the same height of the first peak in the oxygen-oxygen radial distribution function $g_{OO}^{max}(r)$ and the same diffusion coefficient D as the polarizable potential. At all three temperatures studied, λ^* was found to be close to 0.8, i.e. the dipole moment which models the polarizable potential the best is somewhat lower than the average dipole moment found when conducting a simulation using the polarizable potential. It was found that the effective potential in addition to $g_{OO}^{max}(r)$ and D reproduced the molecular rotational relaxation times and the hydrogen bonding properties of the polarizable potential, whereas the dielectric properties and the velocity autocorrelation function were less well reproduced.

VI.3 The dielectric function of benzene

The recent rapid development of powerful and tunable lasers has revolutionized optical spectroscopy, and has been accompanied by the provision of a number of techniques exploiting these devices. One such technique, THz time domain spectroscopy,^{87–89} yields information of the far infrared spectral region dominated by intermolecular interactions. Since such interactions are appropriately investigated by simulation methods, the interpretation of far infrared spectra is often aided by MD simulation results.

The work presented in Paper IX was devoted to the study of the dielectric function of benzene and its temperature and density dependence. The dielectric function is related to the Fourier transform of the total dipole moment time correlation function $C_M(t)$, which was determined from MD simulation and found to agree well with experimental results obtained from THz spectroscopy. To investigate the origin of the dielectric function in detail, advantage was taken from two different partitioning schemes of $C_M(t)$. In (a) the correlation function was partitioned into its contributions from two-, three-, and four-body interactions, and in (b) into a component arising from the correlation of the induced dipole moment of a single molecule and a component arising from the correlation among distinct induced dipole moments. The latter procedure was refined by (c) projecting the induced dipole moments on the molecular axes and subsequently studying the correlation in terms of in-plane, out-of-plane, and cross contributions. The n -body partitioning (a) showed that the temperature dependence of the two- and three-body correlation functions at time zero can be explained solely by density change arguments. Moreover, the ratio of the spectra of these correlation functions in the frequency range 1.8–3.8 THz was found to be constant and temperature independent, indicating that the underlying molecular motion is approximately temperature independent, in contrast to the behavior at lower frequencies. The molecular projection scheme (c) led to concluding that the dielectric loss could be attributed to (i) an out-of-plane libration contributing at all frequencies, completely governing the spectrum above 2 THz, (ii) a small contribution from an in-plane libration below 2 THz, and finally (iii) diffusion below 1 THz. The role of diffusion was, however, found to be very different than that observed for polar liquids. The temperature dependence of the spectra was interpreted in terms of the tempera-

ture dependence of each of these three contributions. The analysis of absorption spectra has elsewhere been conducted in terms of simple molecular reorientation correlation functions C_x and C_z and their pseudo-absorption spectra.⁹⁰ It was established that this method could not be applied in the analysis of the dielectric loss for two reasons: The in-plane libration was found to be exaggerated in the C_x correlation function, and axial correlation was found to persist in C_z after the corresponding dipole moment correlation has vanished.

The extension of these studies, and in particular the novel (c) partitioning scheme, to other liquids should be rewarding. Hexafluorobenzene has almost the same molar density and polarizability as benzene, but the quadrupole moments of hexafluorobenzene and benzene although of similar magnitude have opposite signs. Nevertheless, the absorption of hexafluorobenzene in the far infrared region is significantly lower than that of benzene. Moreover, since the molecular symmetry of benzene is central to the analysis applied here it would be of substantial interest to investigate liquids of similar molecules, but with a different point group symmetry such as *p*-difluorobenzene.

Acknowledgments

The present thesis is a result of my efforts as a Ph.D. student. The work has taken place primarily at The Department of Chemistry at Aarhus University and at Center for Chemistry and Chemical Engineering, Lund University. I wish to extend my gratitude to my supervisors Prof. Kurt V. Mikkelsen and Prof. Jan Linderberg, and further to Dr. Per-Olof Åstrand, Risø National Laboratory and Prof. Per Linse, Lund University to whom I am also very grateful for his extended hospitality during my visits to Lund.

I am also very thankful to have had the opportunity to work with the following people

- Søren Keiding
- Georg K. H. Madsen
- Jens Å. Poulsen
- Cecilie Rønne
- Kristian O. Sylvester-Hvid

Further, I wish to express my gratitude to the following people for their valuable advise and help during the preparation of this thesis.

- Bjørn R. Jensen
- Cecilie Rønne
- Kristian O. Sylvester-Hvid
- Per-Olof Åstrand

Bibliography

- [1] R. A. Horne, *Water and Aqueous Solutions: Structure, Thermodynamics and Transport Processes* (Wiley, New York, 1972).
- [2] J. A. Barker and R. O. Watts, *Chem. Phys. Lett.* **3**, 144 (1969).
- [3] C. H. Cho, S. Singh, and G. W. Robinson, *J. Chem. Phys.* **107**, 7979 (1997).
- [4] M. Born and J. R. Oppenheimer, *Ann. Phys.* **84**, 457 (1927).
- [5] G. D. Billing and K. V. Mikkelsen, *Chem. Phys.* **182**, 249 (1994).
- [6] P. Linse, A. Wallqvist, P.-O. Åstrand, T. M. Nymand, V. Lobaskin, and F. Carlsson, *MOLSIM v. 3.0.7*, Lund University, Sweden, 2000.
- [7] W. F. van Gunsteren, S. R. Billeter, A. A. Eising, P. H. Hünenberger, P. Krüger, A. E. Mark, W. R. Scott, and I. G. Tironi, *Biomolecular Simulation: The GROMOS96 manual and user guide*, Zürich, Switzerland, 1996.
- [8] M. P. Allen and D. S. Tildesley, *Computer Simulations of Liquids* (Clarendon, Oxford, 1987).
- [9] D. van der Spoel, A. R. van Buuren, E. Apol, P. J. Meulenhoff, D. P. Tieleman, A. L. T. M. Sijbers, B. Hess, K. A. Feenstra, E. Lindahl, R. van Drunen, and H. J. C. Berendsen, *Gromacs User Manual version 2.0*, Nijenborgh 4, 9747 AG Groningen, The Netherlands. Internet: <http://md.chem.rug.nl/~gmx>, 1999.
- [10] H. J. C. Berendsen, J. R. Grigera, and T. P. Straatsma, *J. Phys. Chem.* **91**, 6269 (1987).
- [11] L. X. Dang and T.-M. Chang, *J. Chem. Phys.* **106**, 8149 (1997).
- [12] B. Y. Simkin and I. I. Sheikhet, *Quantum Chemical and Statistical Theory of Solutions. A Computational Approach* (Ellis Horwood Lim., London, 1995).
- [13] D. van der Spoel, P. J. van Maaren, and H. J. C. Berendsen, *J. Chem. Phys.* **108**, 10220 (1998).
- [14] S. F. Boys and F. Bernardi, *Mol. Phys.* **19**, 553 (1970).
- [15] I. C. Hayes and A. J. Stone, *Mol. Phys.* **53**, 83 (1984).

- [16] B. Jeziorski, R. Moszynski, and K. Szalewicz, *Chem. Rev.* **94**, 1887 (1994).
- [17] A. D. Buckingham, in *Intermolecular Forces.*, *Adv. Chem. Phys.* **12**, edited by J. O. Hirschfelder (Wiley, New York, 1967).
- [18] C. G. Gray and K. E. Gubbins, *Theory of Molecular Fluids* (Clarendon, Oxford, 1984), Vol. 1.
- [19] A. J. Stone, *The theory of intermolecular forces* (Clarendon Press, Oxford, 1996).
- [20] P.-O. Åstrand, *Hydrogen bonding as described by perturbation theory* Ph.D. thesis, University of Lund, 1994.
- [21] B. H. Bransden and C. J. Joachain, *Physics of atoms and molecules* (Longman, Essex, 1983).
- [22] S. Gasiorowicz, *Quantum physics* (Wiley, New York, 1974).
- [23] F. London, *Z. Physik* **63**, 245 (1930).
- [24] F. London, *Z. Physik. Chem. B* **11**, 221 (1930).
- [25] M. Margenau and N. R. Kestner, *Theory of Intermolecular Forces* (Pergamon, Oxford, 1969).
- [26] A. Wallqvist and G. Karlström, *Chem. Scr.* **29A**, 131 (1989).
- [27] A. Wallqvist, P. Ahlström, and G. Karlström, *J. Phys. Chem.* **94**, 1649 (1990), Erratum in *J. Phys. Chem.* **95**, 4922 (1991).
- [28] O. Engkvist, *Flexible molecular systems studied by quantum chemistry and statistical mechanics* Ph.D. thesis, University of Lund, 1997.
- [29] S. Brdarski, *Modeling of intra- and intermolecular potentials* Ph.D. thesis, University of Lund, 1999.
- [30] P.-O. Åstrand, P. Linse, and G. Karlström, *Chem. Phys.* **191**, 195 (1995).
- [31] D. Frenkel and B. Smit, *Understanding Molecular Simulation* (Academic Press, San Diego, 1996).
- [32] F. Reif, *Fundamentals of statistical and thermal physics* (McGraw-Hill, New York, 1965).
- [33] H. Goldstein, *Classical mechanics*, 2nd ed. (Addison-Wesley Publishing, Reading, Massachusetts, 1980).
- [34] W. H. Press, S. A. Teukolsky, W. T. Vetterling, and B. P. Flannery, *Numerical Recipes* (Cambridge U. P., Cambridge, 1992).
- [35] L. Verlet, *Phys. Rev.* **159**, 98 (1967).

- [36] W. C. Swope, H. C. Andersen, P. H. Berens, and K. R. Wilson, *J. Chem. Phys.* **76**, 637 (1982).
- [37] N. Metropolis, A. W. Rosenbluth, M. N. Rosenbluth, A. H. Teller, and E. Teller, *J. Chem. Phys.* **21**, 1087 (1953).
- [38] P. Ewald, *Ann. Phys.* **64**, 253 (1921).
- [39] H. Kornfeld, *Z. Phys.* **22**, 27 (1924).
- [40] S. W. de Leeuw, J. W. Perram, and E. R. Smith, *Proc. R. Soc. Lond. A.* **373**, 27 (1980).
- [41] H. G. Petersen, *J. Chem. Phys.* **103**, 3668 (1995).
- [42] L. Onsager, *J. Am. Chem. Soc.* **58**, 1486 (1936).
- [43] C. J. F. Böttcher, *Theory of Electric Polarization* (Elsevier, Amsterdam, 1984), Vol. I.
- [44] *MPI: A Message-Passing Interface standard (version 1.1)* Technical report, Message Passing Interface Forum, (1995) , <http://www.mpi-forum.org>.
- [45] *MPI-2: Extensions to the Message-Passing Interface* Technical report, Message Passing Interface Forum, (1997) , <http://www.mpi-forum.org>.
- [46] D. Chandler, *J. Chem. Phys.* **68**, 2959 (1978).
- [47] D. Chandler, *Introduction to Modern Statistical Mechanics* (Oxford University Press, New York, 1987).
- [48] H. Eyring, *J. Chem. Phys.* **3**, 107 (1935).
- [49] J. B. Anderson, *J. Chem. Phys.* **58**, 4684 (1973).
- [50] R. L. Jaffe, J. M. Henry, and J. B. Anderson, *J. Chem. Phys.* **59**, 1128 (1973).
- [51] S. S. Shaik, H. B. Schlegel, and S. Wolfe, *Theoretical Aspects of Physical Organic Chemistry: The S_N2 Mechanism* (Wiley, New York, 1992).
- [52] G. D. Billing, *Chem. Phys.* **159**, 109 (1992).
- [53] G. M. Torrie and J. P. Valleau, *J. Comp. Phys.* **23**, 187 (1977).
- [54] O. Engkvist and G. Karlström, *Chem. Phys.* **213**, 63 (1996).
- [55] H. J. C. Berendsen, J. P. M. Postma, W. F. van Gunsteren, and J. Hermans, in *Intermolecular forces*, edited by B. Pullman (Reidel, Dordrecht, 1981), pp. 331–342.
- [56] W. J. Albery and M. M. Kreevoy, *Advan. Phys. Org. Chem.* **16**, 87 (1987); S. S. Shaik, *J. Am. Chem. Soc.* **106**, 1227 (1984).
- [57] J. Chandrasekhar, S. F. Smith, and W. L. Jorgensen, *J. Am. Chem. Soc.* **107**, 154 (1985).

- [58] M. D. Todd, R. H. Todd, and K. V. Mikkelsen, *J. Mol. Struct.* **314**, 49 (1994).
- [59] J. Tomasi and M. Persico, *Chem. Rev.* **94**, 2027 (1994).
- [60] V. G. Malkin, O. L. Malkina, G. Steinebrunner, and H. Huber, *Chem. Eur. J.* **2**, 452 (1996).
- [61] D. B. Chesnut and B. E. Rusiloski, *J. Mol. Struct.* **314**, 19 (1994).
- [62] B. Pfrommer, F. Mauri, and S. G. Louie, *J. Am. Chem. Soc.* **122**, 123 (2000).
- [63] C. J. Jameson and A. C. de Dios, *J. Chem. Phys.* **97**, 417 (1992).
- [64] I. M. Svishchev and P. G. Kusalik, *J. Am. Chem. Soc.* **115**, 8270 (1993).
- [65] A. D. Buckingham, T. Schaefer, and W. G. Schneider, *J. Chem. Phys.* **32**, 1227 (1960).
- [66] A. D. Buckingham, *Can. J. Chem.* **38**, 300 (1960).
- [67] J. G. Batchelor, *J. Am. Chem. Soc.* **97**, 3410 (1975).
- [68] F. London, *Trans. Faraday Soc.* **33**, 8 (1937).
- [69] G. Karlström, *Theor. Chim. Acta* **60**, 535 (1982).
- [70] G. Karlström, *Theor. Chim. Acta* **55**, 233 (1980).
- [71] A. Rizzo, T. Helgaker, K. Ruud, A. Barszczewicz, M. Jaszuński, and P. Jørgensen, *J. Chem. Phys.* **102**, 8953 (1995).
- [72] J. D. Augspurger, C. E. Dykstra, and E. Oldfield, *J. Am. Chem. Soc.* **113**, 2447 (1991).
- [73] J. D. Augspurger and C. E. Dykstra, *J. Am. Chem. Soc.* **115**, 12016 (1993).
- [74] P.-O. Åstrand and G. Karlström, *Mol. Phys.* **77**, 143 (1992).
- [75] A. D. Buckingham and Y. Tantirungrotechai, *Mol. Phys.* **96**, 1217 (1999).
- [76] M. Pecul, J. Leszczynski, and J. Sadlej, *J. Chem. Phys.* **112**, 7930 (2000).
- [77] T. Helgaker, M. Jaszuński, and K. Ruud, *Chem. Rev.* **99**, 293 (1999).
- [78] A. D. Buckingham and Y. Tantirungrotechai, *Mol. Phys.* **96**, 1225 (1999).
- [79] A. J. Stone, *Mol. Phys.* **56**, 1065 (1985).
- [80] J. G. Ángyán, G. Jansen, M. Loos, C. Hättig, and B. A. Heß, *Chem. Phys. Lett.* **219**, 267 (1994).
- [81] K. O. Sylvester-Hvid, K. V. Mikkelsen, and M. A. Ratner, *J. Phys. Chem. A* **103**, 8447 (1999).

-
- [82] H. A. Lorentz, *The Theory of Electrons*, 2nd ed. (Dover, New York, 1952).
- [83] C. J. F. Böttcher and P. Bordewijk, *Theory of Electric Polarization* (Elsevier, Amsterdam, 1984), Vol. II.
- [84] F. J. Vesely, *J. Comp. Phys.* **24**, 361 (1977).
- [85] A. J. Stone, *Chem. Phys. Lett.* **155**, 102 (1989).
- [86] P. Ahlström, A. Wallqvist, S. Engström, and B. Jönsson, *Mol. Phys.* **68**, 563 (1989).
- [87] J. E. Pedersen and S. R. Keiding, *IEEE J. Quantum. Elec.* **28**, 2518 (1992).
- [88] S. R. Keiding, *J. Phys. Chem. A* **101**, 5250 (1997).
- [89] C. Rønne, K. Jensby, B. J. Loughnane, J. Fourkas, O. F. Nielsen, and S. R. Keiding, to be published in *J. Chem. Phys.*, Volume 113, Issue 9. (unpublished).
- [90] Y. Danten, B. Guillot, and Y. Guissani, *J. Chem. Phys.* **96**, 3782 (1992).